Tectonics

RESEARCH ARTICLE
10.1029/2020TC006429

Key Points:

- Thin-skinned and thick-skinned thrusts record a progressive downward shift in the basal detachment of the Idaho-Montana fold-thrust belt
- A transition from thin-skinned to thick-skinned thrusting occurred as the basal detachment encountered the basement high of the Lemhi arch
- Thin-skinned thrusts in the overlying cover and thick-skinned thrusts below the basement/cover contact form a double-decker fold-thrust belt

Correspondence to:
S. D. Parker,
parkstua@isu.edu

Citation:
Parker, S. D., & Pearson, D. M. (2021). Pre-thrusting stratigraphic control on the transition from a thin-skinned to thick-skinned structural style: An example from the double-decker Idaho-Montana fold-thrust belt. *Tectonics*, *40*, e2020TC006429. https://doi.org/10.1029/2020TC006429

Received 14 JUL 2020
Accepted 4 MAY 2021

Pre-Thrusting Stratigraphic Control on the Transition From a Thin-Skinned to Thick-Skinned Structural Style: An Example From the Double-Decker Idaho-Montana Fold-Thrust Belt

S. D. Parker[1] **and D. M. Pearson**[1]

[1]Department of Geosciences, Idaho State University, Pocatello, ID, USA

Abstract Continental fold-thrust belts display a variety of structural styles, ranging from thin-skinned thrusts following weak lithologic contacts to thick-skinned thrusts that deform mechanical basement. The common practice of splitting fold-thrust belts into thin-skinned and thick-skinned map domains has not yielded a predictive model of the primary controls on structural style. Within the Mesozoic-Paleogene Idaho-Montana fold-thrust belt (44°N-45°N, 112°W-114°W), we identify crosscutting thin-skinned and thick-skinned thrusts within an otherwise thin-skinned map domain. This transition occurs within a thin (~2.5 km) portion of the western Laurentian passive margin, where lower strata pinch out over a prominent basement high (Lemhi arch). Early fold-thrust belt shortening of sedimentary cover rocks was accommodated through detachment folding, followed by east-directed, thin-skinned thrusting along regional-scale faults (Thompson Gulch and Railroad Canyon thrusts). Later, basement and cover rocks were tilted toward the southeast and a basement-involved normal fault was reactivated during thick-skinned thrusting (Radio Tower-Baby Joe Gulch-Italian Gulch thrusts), which accommodated shortening at an oblique angle to and truncated the basal detachment of the older thin-skinned thrusts. This progression from thin-skinned to thick-skinned thrusting occurred >50 km from the foreland, coincident with a regional basement high. Thus, the Idaho-Montana fold-thrust belt is a double-decker system, with upper thin-skinned and lower thick-skinned domains. This double-decker model is applicable to other fold-thrust belts and predicts that the transition from thin-skinned to thick-skinned thrusting occurs where the growing critically tapered wedge can no longer fit within the sedimentary cover rocks and the basal detachment steps down into the structurally lower mechanical basement.

1. Introduction

Continental fold-thrust belts are often modeled as wedges of deformed rock that structurally overlie and are detached from underlying basement rocks (e.g., Armstrong, 1968; Bally et al., 1966; Boyer & Elliott, 1982; Burchfiel & Davis, 1972; Dahlstrom, 1970; Davis et al., 1983; Price & Mountjoy, 1970; Royse et al., 1975). The depth of the basal detachment exerts a fundamental control on the geometry of the orogenic wedge and the magnitude of crustal shortening (e.g., Cook & Varsek, 1994; Erslev, 1993; Lacombe & Bellahsen, 2016; Pfiffner, 2017). However, the primary controls on activation of deep versus shallow basal detachments remain elusive, due in part to the considerable differences among global orogenic belts, both in their geodynamic settings (e.g., peripheral or retroarc position, subduction angle, and convergence rates), crustal architecture, and their protracted pre-thrusting geological histories (e.g., Allmendinger & Gubbels, 1996; Allmendinger et al., 1983; Armstrong, 1968; Burchfiel & Davis, 1975; Erslev, 1993; Kley, 1996; Kley et al., 1999; Kulik & Schmidt, 1988; Lacombe & Bellahsen, 2016; Pearson et al., 2013; Pfiffner, 2006, 2017; Yonkee & Weil, 2015).

The wide varieties of thrust geometries in contractional mountain belts are often assigned to one of two end-member structural styles: thin-skinned or thick-skinned (e.g., DeCelles, 2004; Fitz-Díaz et al., 2018; Kley, 1996; Lacombe & Bellahsen, 2016; McGroder et al., 2015; Molinaro et al., 2005; Pfiffner, 2017; Yonkee & Weil, 2015). Thin-skinned thrusts generally have flat to low-angle upper crustal detachment horizons within weak sedimentary rocks (e.g., Bally et al., 1966; Boyer & Elliott, 1982; Dahlstrom, 1970). Thrusts that cut mechanical basement may be called thin-skinned if they are low-angle and/or have detachment horizons that mostly exploit weak sedimentary rocks (e.g., Pfiffner, 2017; Yonkee & Weil, 2015). In contrast, thick-skinned thrusts deform mechanical basement rocks, cutting across primary lithologic contacts at a

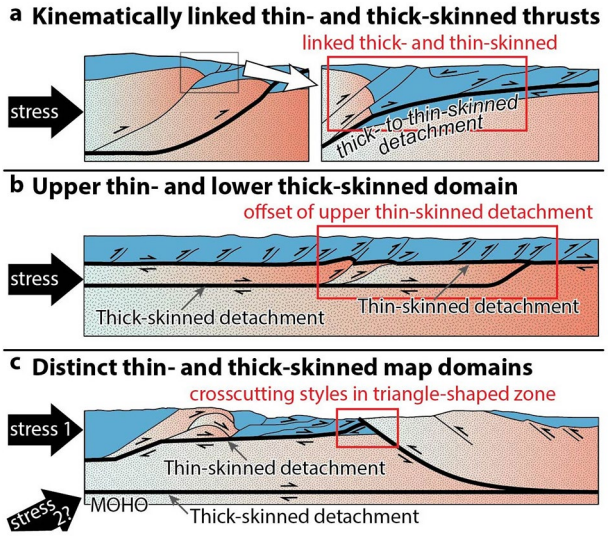

Figure 1. Simplified models showing possible geometric and kinematic overlap of thin-skinned and thick-skinned structural styles. Red boxes call attention to specific areas of overlap. Sedimentary cover rocks (blue) overlie mechanical basement (pink patterns) in all models. (a) Kinematically linked thin-skinned and thick-skinned thrusts are attributed to mechanical properties of pre-thrusting rocks, preexisting weaknesses, and a fixed basal detachment horizon (modified from Giambiagi et al. [2008], [2009], and Fuentes et al. [2016]). (b) A double-decker system is attributed to mechanical properties and transient basal detachment horizons (modified from Molinaro et al. [2005], Mouthereau et al. [2007], and Lacombe & Bellahsen [2016]). (c) Distinct thin-skinned and thick-skinned map domains are attributed to fixed basal detachment horizons and changes in plate boundary geodynamics and resultant changes in regional stresses (modified from Erslev [1993] and Yonkee & Weil [2015]).

moderate to high angle (e.g., Lacombe & Bellahsen, 2016; Pfiffner, 2017). Thick-skinned thrusts often utilize preexisting weaknesses such as foliations or faults, and are generally rooted at mid-crustal or deeper levels (e.g., Allmendinger et al., 1987; Blackstone, 1940; Erslev, 1993; Groshong & Porter, 2019; Kulik & Schmidt, 1988; Lacombe & Bellahsen, 2016; Pfiffner, 2017; Smithson et al., 1979).

Structural style in some fold-thrust belts occurs along a continuum between thin-skinned and thick-skinned endmembers (Butler et al., 2018; Lacombe & Bellahsen, 2016; Pfiffner, 2017). Figure 1 shows examples of this variability, where thin-skinned and thick-skinned styles may occur (a) along a single thrust, (b) at various depths, and/or (c) within distinct but overlapping map domains. Throughout this study, we use the terms thin-skinned and thick-skinned in reference to the two idealized end-members defined above, to highlight important differences in fault geometry. We emphasize that while the structures being discussed are closer to the end-member being referenced, they in fact fall along a continuum of structural style that is dependent on both substrate and fault geometry. Accurate and detailed descriptions of structural style are foundational for predicting where and when basal detachments initiate, which is a prerequisite for developing tectonic models that integrate horizontal shortening of the upper, middle, and lower crust with changes in plate boundary geodynamics.

Critical taper theory offers testable predictions regarding the geometry and kinematics of thin-skinned fold-thrust belts (Davis et al., 1983), but does not apply at depths below the brittle-plastic transition, which are rarely exposed and difficult to image geophysically. For these reasons, studies of orogenic wedges have focused on deformation of the upper crust, generally integrating brittle rheologies for competent and viscous rheologies for weak rocks (see review by Graveleau et al. [2012]). As a consequence, there is much more uncertainty regarding detachment geometries in thick-skinned thrust domains (e.g., Groshong & Porter, 2019; Witte & Oncken, 2020; Zawislak & Smithson, 1981). With some exceptions (e.g., Kulik & Schmidt, 1988; C. A. Williams et al., 1994), the practical result of this problem has been to separate deformation belts into thin-skinned and thick-skinned domains and treat them as separate entities, making it difficult to synthesize results into a single deformation wedge.

Many modern and ancient mountain belts have spatially overlapping regions that are characterized by a spectrum of thin-skinned and thick-skinned structural styles or exhibit a transition in style through time (Figure 1; e.g., Allmendinger & Gubbels, 1996; Fitz-Díaz et al., 2018; Kley et al., 1999; Lacombe & Bellahsen, 2016; Martínez et al., 2020; McGroder et al., 2015; Pearson et al., 2013; Pfiffner, 2017; S. A. Williams et al., 2020; Yonkee & Weil, 2015). In the southern Subandean fold-thrust belt of the central Andes, the thin-skinned fold-thrust belt was carried atop and transitions along-strike southward to a basement-involved, thick-skinned fold-thrust belt (e.g., Kley, 1996). Farther south in the Andes of west-central Argentina, early thin-skinned structures formed at structurally shallow levels and were subsequently deformed during thick-skinned inversion of structural deeper, basement-involved faults (Figure 1a; Fuentes et al., 2016; Giambiagi, Bechis, et al., 2008). A shallow thin-skinned and deeper thick-skinned fold-thrust belt have been documented in the Zagros (Figure 1b; e.g., Barnhart et al., 2018; Molinaro et al., 2005; Mouthereau et al., 2007). In contrast to these "double-decker" fold-thrust belts, thin-skinned and thick-skinned structures in the Sevier-Laramide fold-thrust belt of the North American Cordillera were often considered by earlier workers to occupy geographically separate regions, with limited spatial and temporal overlap between them (e.g., Armstrong, 1968; Burchfiel & Davis, 1975; Dickinson & Snyder, 1978). However, more recent study in the North American Cordillera has shown that thin-skinned thrusts overlapped in time with or were deformed by later, structurally deeper, thick-skinned thrusts (e.g., Fitz-Díaz et al., 2018; O'Neill et al., 1990; Ramírez-Peña

& Chávez-Cabello, 2017; Schmidt & Perry, 1988; S. A. Williams et al., 2020; Yonkee & Weil, 2015; Zhou et al., 2006). Overlap of structural styles has primarily been documented near the foreland, leading to the interpretation of distinct thin-skinned and thick-skinned thrust domains that converge toward one another, each with a unique basal detachment and possibly stress field (Figure 1c; e.g., Erslev, 1993; Jordan & Allmendinger, 1986; Yonkee & Weil, 2015). Alternatively, the North American Cordillera may qualify as a "double-decker" fold-thrust belt, with a continuum of thin-skinned to thick-skinned structural styles that not only vary across and along strike, but also with depth (cf., Lacombe & Bellahsen, 2016; Pfiffner, 2017).

To evaluate these models and investigate what controls the activation of deep versus shallow basal detachments, the spatial relationship between structural domains must be well-constrained (e.g., Giambiagi et al., 2012). Where the interaction between basal detachments of thin-skinned thrusts and underlying thick-skinned structures is observable, we can begin to construct a more representative three-dimensional view of the boundary separating structural domains and test whether the depth, relative strength, orientation, and/or continuity of the preexisting stratigraphy correlates with changes in structural style. Within the Idaho-Montana segment of the Sevier-Laramide fold-thrust belt (Figure 2), both end-member structural styles have been documented and a wide range of structural levels are exposed in a relatively small, accessible area (e.g., Kulik & Schmidt, 1988; McDowell, 1997; O'Neill et al., 1990; Perry, Dyman, & Sando, 1989; Perry et al., 1988; Schmidt, O'Neill, & Brandon, 1988; Skipp, 1988; Tysdal, 1988, 2002). In the central part of the fold-thrust belt, erosion has fortuitously removed upper structural levels, creating a window into footwalls of thin-skinned thrusts. The study area is far from the foreland (Figure 2), in a region that most previous workers have assumed is not thick-skinned despite the common outcrops of mechanical basement. Through mapping and structural analysis, we constrain thrust geometries and interpret the series of deformation events that involve both thin-skinned and thick-skinned thrusts near the contact between mechanical basement and overlying sedimentary rocks. Our results suggest that episodes of thin-skinned and thick-skinned shortening overlapped in space and time and that the primary control on structural style was pre-thrusting variations in thickness and lateral continuity of regional stratigraphic detachment horizons. These results provide a predictive framework for linking variable structural styles at various depths to a single deformation belt, suggesting that basal detachment horizons to continental fold-thrust belts are not fixed and instead migrate downward through the mechanically stratified crust with progressive shortening.

2. Background

2.1. Controls on Structural Style

In the shallow crust, the mechanical stratigraphy within a fold-thrust belt exerts a fundamental control on the geometries of its constitutive structures (Rich, 1934). Strength contrasts within sedimentary rocks promote ramps and flats, imbricate fans, and duplexes, which shorten cover rocks that are decoupled from the underlying mechanical basement (e.g., Boyer & Elliott, 1982; Rich, 1934; Stockmal et al., 2007). Classic localities exhibiting this thin-skinned structural style include the Canadian Rockies (Bally et al., 1966; Dahlstrom, 1970; Fermor & Moffat, 1992; McMechan et al., 1993; Price, 1981), Wyoming salient of the Sevier thrust belt (Armstrong, 1968; Burchfiel & Davis, 1972; Coogan, 1992; DeCelles, 1994; DeCelles & Coogan, 2006; DeCelles & Mitra, 1995; Wiltschko & Dorr, 1983; Yonkee & Weil, 2010, 2015), and the Subandean fold-thrust belt of the central Andes (Allmendinger et al., 1983; Baby et al., 1995; Dunn et al., 1995; Echavarria et al., 2003; Fuentes et al., 2016; Kley, 1996; Kley et al., 1999; McGroder et al., 2015; McQuarrie, 2002).

Deeper in the crust, we define mechanical basement as rocks that lack sub-horizontal, weak lithological layers that are exploited during thin-skinned thrusting. Rocks that we characterize as mechanical basement rocks are previously deformed, metamorphic, or plutonic rocks from prior tectonism. Whereas sedimentary cover rocks utilize pre-thrusting, weak lithologic layers as subhorizontal detachment horizons (e.g., Rich, 1934), mechanical basement rocks do not break along primary lithologic contacts. Instead, mechanical basement often breaks along inherited weaknesses, leading to a wide range in orientations and dip angles of reverse faults. Our usage of terms highlights that while all rocks tend to exploit preexisting weaknesses, in the upper crust these weaknesses tend to be subhorizontal for sedimentary cover rocks and in a variety of orientations for mechanical basement rocks, resulting in the observed range of thin-skinned to thick-skinned structural styles.

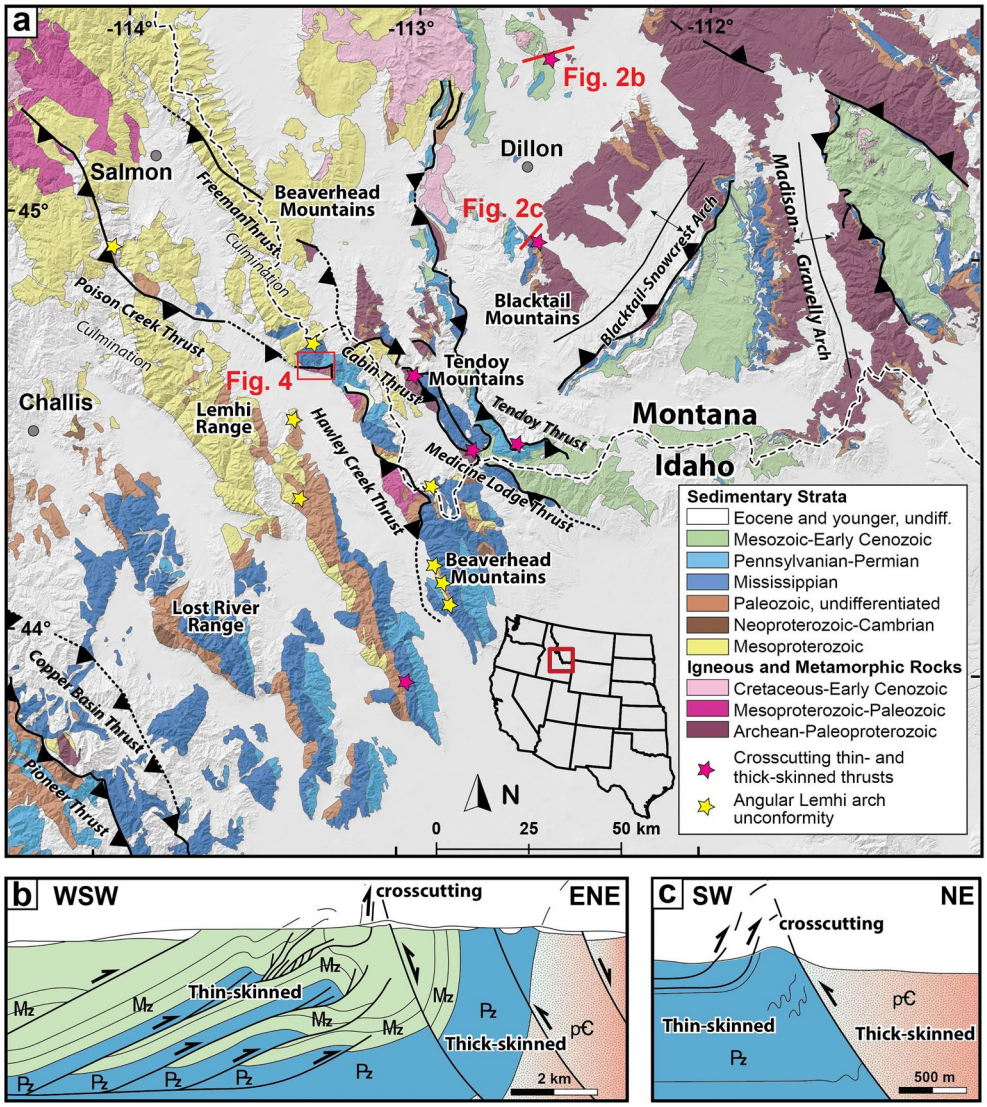

Figure 2. (a) Simplified bedrock geologic map of the Idaho-Montana fold-thrust belt showing major thrusts (modified from Garber et al. [2020]). Pink stars show where crosscutting thin-skinned and thick-skinned thrusts have been previously documented (see text for discussion and citations). Yellow stars show where the Lemhi arch unconformities have a discordance of >10° (James & Oaks, 1977; Pearson & Link, 2017; Ruppel, 1986; Scholten, 1957; Scholten & Ramspott, 1968). Schematic cross-sections showing crosscutting relationship between thin-skinned and thick-skinned thrusts in the (b) McCartney Mountain salient (redrafted from Schmidt, O'Neill, & Brandon [1988]) and (c) Blacktail Mountains (redrafted from Tysdal [1988]).

In contrast to thin-skinned thrusts, thick-skinned thrusts generally carry thicker thrust sheets of mechanical basement rocks. These thrusts are often listric and merge into the middle to lower crust, where temperature-dependent strength contrasts likely separate regions that deform by frictional versus plastic mechanisms and may therefore be utilized as subhorizontal detachment horizons (Erslev, 1993; Kulik & Schmidt, 1988; Lacombe & Bellahsen, 2016; Mouthereau, Watts, & Burov, 2013). Though thick-skinned systems may have detachments at various depths down to the lower crust (depending on the temperature and composition of the lithosphere), these faults do not cut the entire lithosphere (e.g., Erslev, 1993; Lacombe & Bellahsen, 2016; McBride et al., 1992; Richardson et al., 2013; Smithson et al., 1979; Worthington et al., 2016; Yeck et al., 2014). During thrusting, as basement rocks are translated from subhorizontal detachment horizons over ramps in the upper crust (Figure 1; e.g., Erslev, 1993), crowding at high structural levels may result in the formation of synthetic and antithetic thick-skinned thrusts (e.g., Erslev, 1986; Gray

et al., 2019; Groshong & Porter, 2019). Given that thin-skinned thrusts utilize weak lithologies within the upper crust and thick-skinned thrusts are thought to utilize subhorizontal strength contrasts within the middle and lower crust, thin-skinned and thick-skinned domains may occur in the same area but at different structural depths (Betka et al., 2015; Kulik & Schmidt, 1988; Lacombe & Bellahsen, 2016).

In some fold-thrust belts, including in a few localities within the Sevier fold-thrust belt, slivers of mechanical basement can be incorporated into structural culminations (Boyer & Elliott, 1982; DeCelles, Lawton, & Mitra, 1995; O'Sullivan & Wallace, 2002; Pfiffner, 2006, 2017; Yonkee, 1992). In the North American Cordillera, formation of these anticlinoria was likely controlled by the basement step at the eastern limit of thick Neoproterozoic strata within the western Laurentian rift margin (Figure 1c; Carney & Janecke, 2005; DeCelles, 1994, 2004; DeCelles & Coogan, 2006; Long, 2012; Yonkee, 1992). Regional-scale basement slivers can also be found in structurally deep portions of fold-thrust belts where the brittle-plastic transition occurs directly below the basement-cover contact (e.g., Lacombe & Bellahsen, 2016; Pfiffner, 2017). In our view, these basement-involved thrusts represent a transitional example in the continuum between thin-skinned and thick-skinned structural styles, because basement is not fundamentally involved in shortening and basement deformation is facilitated by plastic—not frictional—deformation mechanisms (e.g., Yonkee, 1992).

Critical taper theory serves as a foundation for understanding how deformation propagates through a thin-skinned fold-thrust belt (Davis et al., 1983), but is less clearly applied to thick-skinned domains. In the critical taper model, horizontal shortening is accommodated by vertical thickening of the crust; during continued shortening, the locus of active deformation propagates away from the thickened region, creating a wedge-shaped fold-thrust belt. Thickening within the wedge increases the taper angle (dip of the basal detachment plus surface slope) beyond the critical value set by the compressive strength of the material within the wedge and the frictional resistance to sliding at the base of the wedge. In response, the thrust front propagates forward, surface slope decreases to subcritical conditions, and internal thickening resumes. Deformation of the wedge alternates between forward propagation of "in-sequence" thrusts and internal thickening during "out-of-sequence" thrusting. Crucially, critical taper models assume that a single, fixed basal detachment is utilized throughout the deformation of the wedge.

In natural orogenic wedges, the basal detachment cuts up-section in the direction of transport and migrates forward through time (Boyer & Elliott, 1982; Dahlstrom, 1970), advancing when the wedge is in a supercritical state of taper (Davis et al., 1983). Slip is often transferred from the basal detachment to stratigraphically higher detachment horizons (including within foreland basin sedimentary rocks; Chapman & DeCelles, 2015) and eventually to the surface. As the orogenic wedge continues to propagate, slip along the frontal thrust wanes as the basal detachment begins to carry the former toe thrust in its hanging wall and feeds slip into a newly initiated frontal thrust. This results in sequential down-stepping of the frontal thrust to the basal detachment through time, which is widely documented globally, including in the Sevier fold-thrust belt (e.g., Royse et al., 1975), the Himalayan fold-thrust belt (e.g., DeCelles, Robinson, et al., 2001), and the central Andean fold-thrust belt (e.g., Echavarria et al., 2003).

Thick-skinned thrusts are generally not interpreted within the context of critical taper theory because their level of detachment (if any) is often unknown and is likely below the brittle-plastic transition, the large thrust spacing complicates approximations of the surface slope, and pre-existing weaknesses are often reactivated (e.g., Erslev, 1993; Groshong & Porter, 2019; Pearson et al., 2013). Models of thick-skinned thrust belts generally predict that the basal detachment utilizes strength contrasts, either becoming subhorizontal near the brittle-plastic transition (e.g., Armstrong & Dick, 1974; Kulik & Schmidt, 1988), or continuing to deeper levels (Erslev, 1993; Mazzotti & Hyndman, 2002; McQueen & Beaumont, 1989; Scheevel, 1983), depending on the temperature-dependent strength profile of the lithosphere (Lacombe & Bellahsen, 2016). Regardless of scale, modeling demonstrates that strength contrasts determine not only detachment horizons, but also the structural style (Bauville & Schmalholz, 2015; Ruh et al., 2012; Simpson, 2010; Stockmal et al., 2007). In the upper crust, thick-skinned thrust systems may also utilize pre-thrusting weaknesses such as basement foliations (e.g., Schmidt et al., 1995) or shear zones (Weil, Yonkee, & Kendall, 2014), dikes (e.g., Neely & Erslev, 2009), or older normal faults (e.g., Pearson et al., 2013).

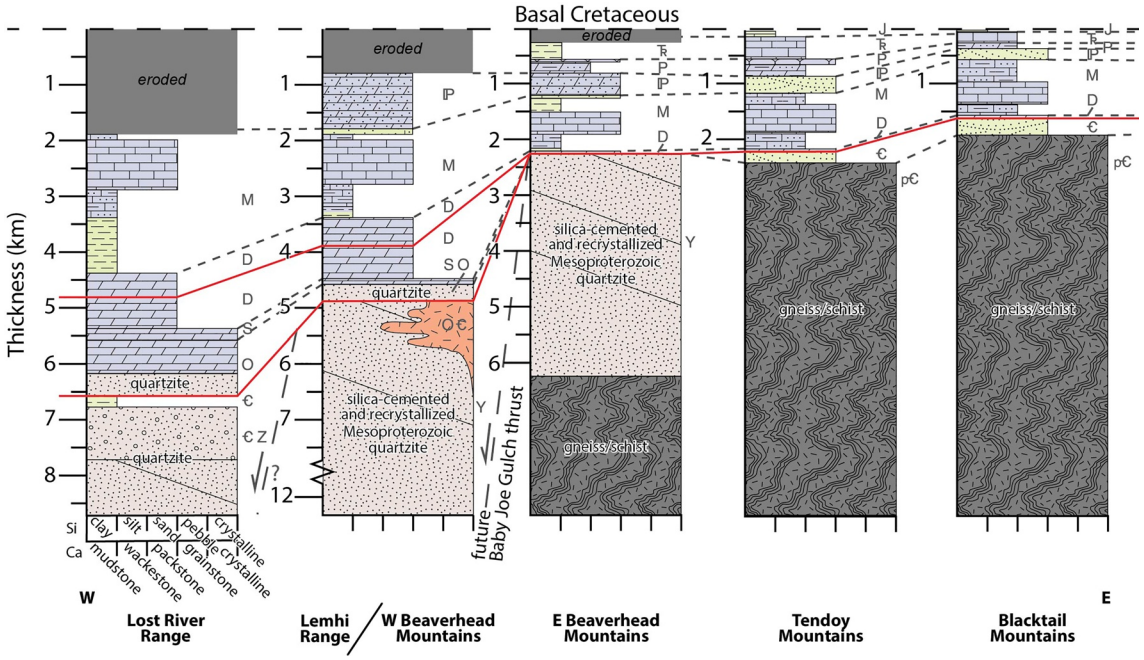

Figure 3. Generalized lithostratigraphic columns across the Idaho-Montana fold-thrust belt (see Figure 2 for locations). Red lines show sub-Ordovician and intra-Devonian Lemhi arch unconformities (Grader et al., 2017), with angular unconformities shown where appropriate. Lithologies and grain sizes for siliciclastic (Si) and carbonate (Ca) units are shown on *x*-axis. Blue represents carbonate units; green represents poorly cemented siliciclastic units; tan represents quartzites. Approximate thicknesses are shown below a datum at the base of Cretaceous strata (or younger rocks, depending on erosion level). Generalized correlations of time periods and inferred normal faults are shown as dashed lines.

2.2. Mechanical Stratigraphy of the Idaho-Montana Fold-Thrust Belt

Deformation within the thin-skinned Sevier fold-thrust belt coincides with the gradual westward thickening of sedimentary rocks of the Neoproterozoic and Paleozoic rift and passive margin succession (Burchfiel & Davis, 1975). A hinge line separates thinner stratigraphy overlying the craton in the east from stratigraphy of the carbonate shelf, which thickens toward the west (Huh, 1967; Kay, 1951). The basal detachment for much of the Sevier fold-thrust belt commonly exploited mechanically weak, fine-grained Neoproterozoic and Cambrian rocks that occur near the base of the sedimentary sequence, particularly west of the hinge line (Armstrong, 1968; DeCelles & Coogan, 2006; Price, 1981; Royse et al., 1975; Yonkee & Weil, 2015). Basement heterogeneities near the hinge line resulted in local involvement of mechanical basement, such as is documented in the Wasatch anticlinorium (Yonkee, 1992).

In its northward projection into east-central Idaho and Montana, the lower part of the sedimentary sequence is disrupted by significant along-strike and across-strike facies and thickness changes. Near the interior of the fold-thrust belt, in the Lemhi and Lost River ranges of east-central Idaho (Figure 2), 5–6 km of predominantly pre-orogenic carbonate shelf strata overlie Mesoproterozoic quartzite (Scholten & Hait, 1962; Shannon, 1961; Skipp & Hait, 1977). Around 75 km to the northeast, near the frontal thin-skinned Tendoy thrust and adjacent thick-skinned thrusts of the foreland (Figure 2), a 2–3 km thick Cambrian to Triassic, pre-orogenic section of mixed siliciclastic and carbonate strata (Figure 3) overlies crystalline basement rocks of the craton (Lonn et al., 2000; Skipp, 1988). The study area is within the central Beaverhead Mountains (Figures 2 and 3) between the western carbonate shelf and eastern craton sections (Huh, 1967; Rose, 1976), where a ~2.5 km thick section of Devonian to Pennsylvanian carbonate and mixed siliciclastic strata (Lonn et al., 2019; Lund, 2018; Ruppel, 1968) unconformably overlies a thick, previously tilted succession of fine-grained Mesoproterozoic quartzite (Lonn et al., 2019).

West of the study area, the thickness of Ordovician to Devonian carbonate rocks increases from <200 m in the Lemhi Range to >1 km in the Lost River Range (Figures 2 and 3) (Ross, 1947; Sloss, 1954). The area of thinner stratigraphy was termed the Lemhi arch by Sloss (1954) and interpreted as a positive topographic element during early-Paleozoic to mid-Paleozoic time. Two main unconformities define the basement high:

(a) the sub-Ordovician Lemhi arch unconformity, defined below the Middle Ordovician Kinnikinic Quartzite and (b) the intra-Devonian Lemhi arch unconformity, defined below the upper part of the Late Devonian Jefferson Formation (Figure 3). The sub-Ordovician Lemhi arch unconformity is observable throughout much of the Lemhi and Beaverhead ranges, where Kinnikinic Quartzite overlies Mesoproterozoic quartzite and hypabyssal ~500 Ma Beaverhead plutons (Link et al., 2017; Lund et al., 2010) often with an angularity of 20°–30° (Hansen & Pearson, 2016; Pearson & Link, 2017; Scholten, 1957). The intra-Devonian Lemhi arch unconformity is exposed in the central and southern Beaverhead Mountains, where a thin (<50 m) upper Jefferson Formation rests on Mesoproterozoic quartzite (Grader et al., 2017; Lonn et al., 2019; Scholten & Hait, 1962). The thinning and pinching out of pre-thrusting stratigraphy near the Lemhi arch basement high restricted the distribution of weak layers available for thin-skinned thrusting during Mesozoic time.

2.3. Structural Styles of the Idaho-Montana Fold-Thrust Belt

The fold-thrust belt of east-central Idaho and southwestern Montana (44°N-45°N) forms a prominent reentrant between the Helena salient of central Montana and the Wyoming salient of southeastern Idaho, Wyoming, and northern Utah. In central Idaho (Figure 2), the Pioneer and Copper Basin thrusts form the orogenic interior of an east-verging to northeast-verging, leading imbricate fan (Dover, 1981; Rodgers & Janecke, 1992; Skipp & Hait, 1977). Recent work (Brennan et al., 2020) demonstrates that these thrusts deformed a relatively thick succession of Neoproterozoic and Paleozoic rift and passive margin rocks southwest of the Lemhi arch basement high.

Northeast of the Pioneer and Copper Basin thrusts (Figure 2) is a broad region where no major thrust faults are mapped; instead, large (>15 km wavelength) folds affected Mesoproterozoic quartzites at deeper structural levels (Hansen & Pearson, 2016; Lonn et al., 2016; Tysdal, 2002), structurally below a more tightly folded passive margin succession (Beutner, 1968; Hait, 1965). Northeast of this folded domain, major thrusts include (from west to east) the Hawley Creek, Cabin, Medicine Lodge, and Tendoy thrusts (Lucchitta, 1966; Scholten et al., 1955; Skipp, 1988; Skipp & Hait, 1977). The Cabin and Hawley Creek thrusts are interpreted as along-strike equivalents or footwall imbricates of the Freeman and Poison Creek thrusts, respectively (Figure 2; Evans & Green, 2003; Lonn et al., 2016; Skipp, 1988). In most exposures, these moderately dipping thrusts cut indiscriminately across lithologic contacts within the Mesoproterozoic quartzites and older gneisses and schists that define the Lemhi arch basement high (Hansen & Pearson, 2016; Lonn et al., 2016; Skipp, 1988). Northeast of these mechanical basement-involved thrusts, the Medicine Lodge, Tendoy, and minor related thrusts form an imbricate fan that involves mostly Paleozoic to Mesozoic rocks, including syntectonic wedge-top conglomerates of the foreland basin (Perry & Sando, 1982).

The foreland of southwestern Montana marks the northwesternmost extent of the structurally defined Laramide province, where variably oriented thick-skinned thrusts involve crystalline basement of the craton (Dickinson & Snyder, 1978; Eardley, 1963; Yonkee & Weil, 2015). At upper structural levels throughout the Idaho-Montana fold-thrust belt, including the foreland, middle Paleozoic, and younger carbonate rocks accommodated shortening primarily by folding and bedding-parallel detachment (Anastasio et al., 1997; Ruppel & Lopez, 1988; Tysdal, 1988). Despite the regional continuity of folds and thrusts at these upper structural levels, most prior workers define the Tendoy thrust as the leading edge of the Sevier belt (DeCelles, 2004; Scholten et al., 1955; Skipp, 1988; Skipp & Hait, 1977) and the inferred boundary between thin-skinned and thick-skinned thrust domains.

In the Idaho-Montana fold-thrust belt, interactions among thin-skinned and thick-skinned thrusts can be directly observed. We highlight key areas (pink stars in Figure 2) that illustrate a regional trend of overlapping thin-skinned and thick-skinned thrusts. On the flank of the Blacktail-Snowcrest uplift, thin-skinned thrusts detached in Mississippian rocks are truncated by the thick-skinned Jake Canyon thrust (Figure 2c: Schmidt, O'Neill, & Brandon, 1988; Tysdal, 1988). Similarly, the thin-skinned, east-vergent McCartney Mountain salient (McCarthy Mountain salient of Brumbaugh and Hendrix [1981] and O'Neill et al. [1990]) is cut by or buttressed against the thick-skinned Biltmore anticline (Figure 2b; Lopez & Schmidt, 1985; Schmidt, O'Neill, & Brandon, 1988). Folding related to blind thick-skinned thrusts beneath the thin-skinned Tendoy thrust occurred both before and after slip along the Tendoy thrust (McDowell, 1997; Perry et al., 1988). These examples highlight a regional trend of contemporaneous thin-skinned and thick-skinned thrusts, one on top of the other (Kulik & Schmidt, 1988).

Observations of crosscutting and overlapping structural styles are not confined to the foreland of the Idaho-Montana fold-thrust belt. Most notably, the basement-involved Cabin thrust truncates the thin-skinned Medicine Lodge thrust in the Tendoy and Beaverhead Mountains (Figure 2a; Skipp, 1988). Farther west in the Lemhi and Lost River ranges, structural style changes noticeably with depth (e.g., Kuntz et al., 1994). An upper folded package defines an east-verging fold belt in the Lemhi Range, which is detached within anhydrite-bearing dolostones and shales at the intra-Devonian Lemhi arch unconformity (Beutner, 1968; Hait, 1965). This fold belt is offset and folded by thrusts that cut quartzites and massive dolostones below the intra-Devonian Lemhi arch unconformity. A regional anticline (Patterson culmination of Janecke et al. [2000]) exposes Mesoproterozoic quartzites of the Lemhi arch in its broken core, with the tilted fold belt visible on its flank. Across the region, thrusts that cut quartzite, gneiss, and schist generally have short fault segments that vary from ~NW-SE to ~E-W striking, with moderate to steep dips (Beutner, 1968; Hait, 1965; Lucchitta, 1966; M'Gonigle 1993, 1994; Scholten & Ramspott, 1968; Skipp, 1988), similar to the thick-skinned thrusts of the Montana foreland (e.g., Schmidt & Garihan, 1983; Schmidt, O'Neill, & Brandon, 1988). In summary, throughout the Idaho-Montana fold-thrust belt, thin-skinned thrusts with basal detachments in weak Paleozoic units are overprinted by deeper structures within the mechanical basement of the Lemhi arch.

The absolute age of deformation within these two packages is less constrained. A basal angular unconformity, isopach maps, and reconstructed paleocurrent data from the lower-Cretaceous to mid-Cretaceous Kootenai Formation in the southwestern Montana foreland may suggest early, low-magnitude exhumation related to thick-skinned thrusting (Decelles, 1986; Scholten, 1982; Schwartz, 1982), but within a regionally continuous foreland basin setting with extrabasinal sources (Rosenblume et al., 2021). Provenance studies of the Late Cretaceous to Paleocene Beaverhead Group (Garber et al., 2020; Haley et al., 1991; Perry & Sando, 1982; Ryder & Scholten, 1973) and low-temperature thermochronologic data (Carrapa et al., 2019) suggest mid to Late Cretaceous exhumation of the Blacktail-Snowcrest arch, followed by in-sequence slip along the thin-skinned Medicine Lodge and Tendoy thrusts. Similar observations and interpretations were made for the Hawley Creek and neighboring thrusts, which truncate an open, SW-plunging syncline (Lucchitta, 1966). These observations show a common relationship: thin-skinned thrusts and related folds are mutually crosscutting with deeper thick-skinned structures within the Idaho-Montana fold-thrust belt. Direct exposure of cross-cutting thin-skinned and thick-skinned thrusts thus makes the Idaho-Montana fold-thrust belt a suitable locality for investigating the influence of preexisting stratigraphy on progressive deformation and how a wide variety of structural styles can arise from one protracted shortening event.

3. Methods

In this study, we evaluate the hypothesis that an upper thin-skinned and lower thick-skinned thrust domain are separated by a low-angle basement/cover contact that defines the Lemhi arch (Figure 1b). To test this hypothesis we mapped the northern portion of the Leadore quadrangle (Figure 4) at the 1:24,000-scale (Parker & Pearson, 2020), in the process, documenting the range of structural styles present, their spatial and temporal relationships, and the stratigraphy involved. As a starting point, we used the stratigraphic framework established in the neighboring Bannock Pass quadrangle (Lonn et al., 2019) to the north and placed Devonian rocks in the regional context established by Grader et al. (2017). By comparing local and regional stratigraphy (Figure 3), we constrain the position of the Lemhi arch basement high. We then interpret the deformation features of the study area in a Lemhi arch reference frame.

Field measurements of bedding, foliations, cleavage planes, stretching lineations, and fold hinges were plotted on equal-area, lower hemisphere stereographic projections using the program Stereonet (v. 10.1.6 of Allmendinger, Cardozo, & Fisher, 2013); Kamb contouring at 2σ-uncertainty levels was performed to identify patterns (Mardia, 1972). We quantified patterns as clustered (P) or girdled (G), following methods of Vollmer (1990). After calculating eigenvectors (λ_1, λ_2, and λ_3) in Stereonet, we calculated the proportions that are classified as clustered ($P = \lambda_1 - \lambda_2$) and girdled ($G = 2(\lambda_2 - \lambda_3)$). The remaining proportion (R) assesses the part of the distribution that is random ($R = 3(\lambda_3)$). All P, G, and R values are reported as percentages. For girdled distributions, Bingham statistics were used to calculate the cylindrical best fits of plotted points. For clustered distributions, mean vectors and associated $\pm 2\sigma$ confidence cones were calculated using Fisher vector distributions. When clustered trends overlapped the margin of the plot, we manually rotated the

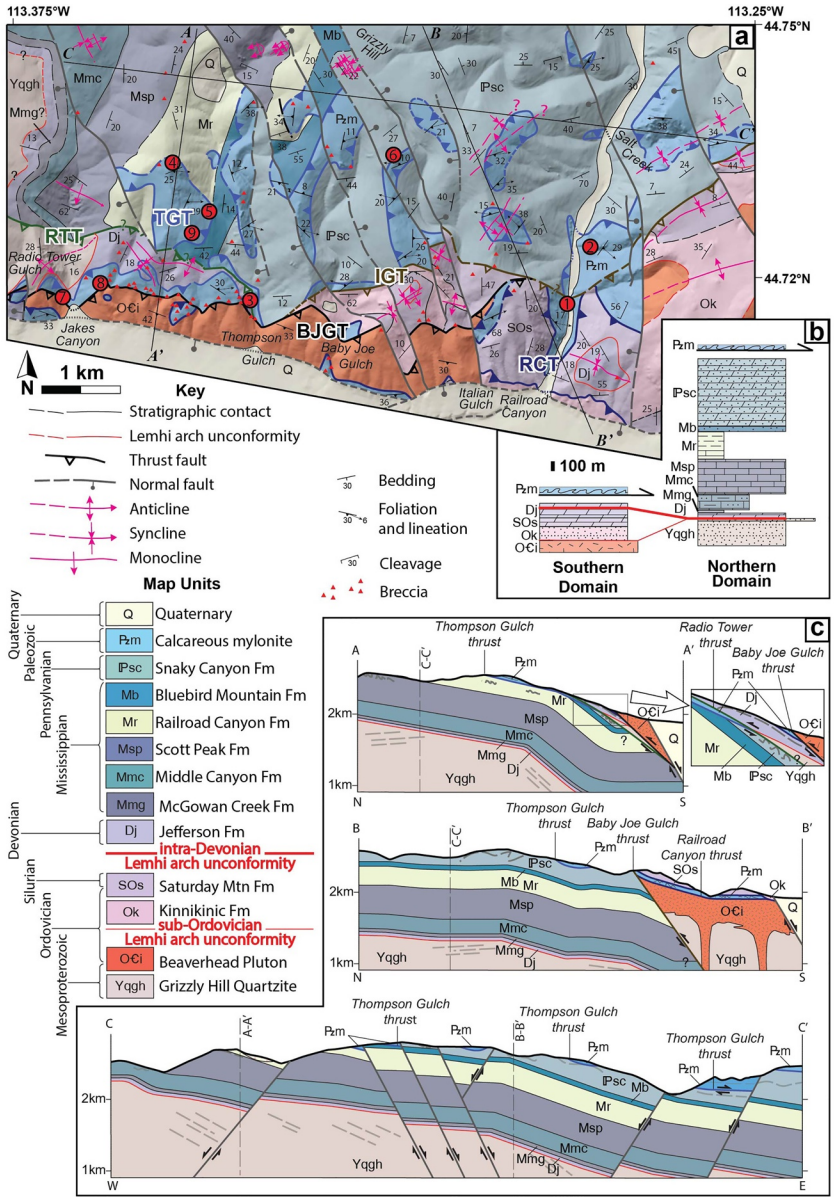

Figure 4. (a) Simplified bedrock geologic map of the study area (see Figure 2 for location; modified from Parker & Pearson [2020]). Thrust faults: RTT = Radio Tower thrust, TGT = Thompson Gulch thrust, BJGT = Baby Joe Gulch thrust, IGT = Italian Gulch thrust, RCT = Railroad Canyon thrust. Numbers in red circles denote specific outcrops referenced in the text. (b) Stratigraphic columns of the southern and northern domains. Red lines denote sub-Ordovician and intra-Devonian Lemhi arch unconformities. (c) Simplified cross-sections.

data to fit in one frame of view before calculating the mean vector. The azimuths of fold hinges were plotted using rose diagrams and a mean vector and the associated $\pm 2\sigma$ confidence interval was calculated using Krumbein's mean vector (Krumbein, 1939).

We documented kinematic indicators of faults and shear zones in the field and in oriented thin sections. Where observed, we measured lengths and heights of rugose corals as viewed in cross-section and lengths and widths of crinoid ossicles as viewed along a common plane of view. In general, cross-sections of strained corals have long axes parallel to cleavage and short axes approximately perpendicular to cleavage. Deformed crinoid ossicles were observed within shear zones and generally exhibited long axes that are approximately parallel to stretching lineations when viewed on the shear foliation surface. We calculated aspect ratios for each measured coral and crinoid, and mean values for all. Uncertainty values reflect the standard deviation

(2σ) of all calculated aspect ratios (length/height) used to calculate the mean. These aspect ratios only approximate the amount of strain within the plane of view. Uncertainty regarding the initial lengths and orientations of strain markers in the field precluded a quantitative determination of the shape of the strain ellipsoid.

We established relative timing constraints from crosscutting relationships observed in the field and inferred from map relationships. Using this relative timeline, we constructed a series of deformation events that relate the preexisting stratigraphy to the resultant structural style by synthesizing our mapping results, measurements of deformation features, and kinematic constraints.

4. Results

4.1. Pre-Thrusting Stratigraphy

Our mapping results corroborate previous interpretations (Lund, 2018; Ruppel, 1968) that two unique stratigraphic packages are exposed in the northern and southern portions of the map area (Figure 4b). We identify previously unrecognized calcareous mylonites overlying both stratigraphic packages.

Approximately 1.8 km of Devonian to Pennsylvanian shelf strata are exposed in the northern portion of the map area (Figure 4; thicknesses walked in the field and measured from geologic map). The Mesoproterozoic Quartzite of Grizzly Hill is the lowest exposed unit. We interpret the age of this unit as Mesoproterozoic and not Cambrian to Mesoproterozoic (Lonn et al., 2019; Parker & Pearson, 2020) because all available detrital zircon dates are Mesoproterozoic in age and we were unable to find conclusive evidence of trace fossils in the field. Above the Quartzite of Grizzly Hill, <50 m of unfossiliferous laminated dolostone of the Devonian upper Jefferson Formation marks the intra-Devonian Lemhi arch unconformity. The overlying Mississippian section consists of (from bottom to top) 28 m of claystone to siltstone and silty lime mudstone of the McGowan Creek Formation, ~600 m of thin-bedded to massive limestone and chert of the Middle Canyon and Scott Peak formations, and ~250 m of lime mudstone, siltstone, and shale of the Railroad Canyon Formation. Above is >850 m of thinly bedded chert and limestone interbedded with calcareous-cemented quartz arenite of the Mississippian to Pennsylvanian Bluebird Mountain and overlying Snaky Canyon formations.

Distinct stratigraphy of the southern portion of the map area is exposed in the hanging walls of thrusts (Figures 4a and 4b). In this stratigraphic package, the Cambro-Ordovician Beaverhead pluton is the lowest exposed unit and is overlain in inferred nonconformity (sub-Ordovician Lemhi arch unconformity) by the cliff-forming Ordovician Kinnikinic Quartzite. Above lies ~250 m of fossiliferous dolostones that are assigned to the Middle Ordovician-Silurian Saturday Mountain and the Late Devonian Jefferson formations based on the fossils *Halysites* and *Amphipora* (Ross, 1934; Stearn, 1997; Stock, 1990).

Map relationships and detailed stratigraphy (Grader et al., 2017) require that before Mesozoic shortening, Devonian and younger strata were laterally continuous across the study area above the intra-Devonian Lemhi arch unconformity, but Ordovician to Devonian strata above the sub-Ordovician Lemhi arch unconformity are confined to the southern part of the map area. The spatial overlap of both unconformities in the study area constrains the specific locations of the Lemhi arch basement high, which is locally composed of the Quartzite of Grizzly Hill and the Beaverhead pluton.

4.2. Structural Domains

The stratigraphic section exposed in the northern part of the study area is part of a >20 km long SE-dipping homocline (Lonn et al., 2019), structurally beneath the stratigraphically different southern area (Figure 4). To simplify the discussion, we separate the study area into three structural domains: (a) the sedimentary rock dip panel, (b) the carbonate mylonite, and (c) the basement-rooted domains. The sedimentary rock dip panel domain includes strata that is both north of the Radio Tower, Baby Joe Gulch, and Italian Gulch thrusts and in the footwall of the Thompson Gulch Thrust. The sedimentary rock dip panel domain is visible on the map (Figure 4) as the SE-dipping homocline that exposes the full Mesoproterozoic to Pennsylvanian section. The carbonate mylonite domain includes rocks in the hanging walls of the Thompson Gulch and Railroad Canyon thrusts. The carbonate mylonite domain is visible on the map as a series of low-angle klippen that overlies both the sedimentary rock dip panel and basement-rooted domains. The basement-rooted

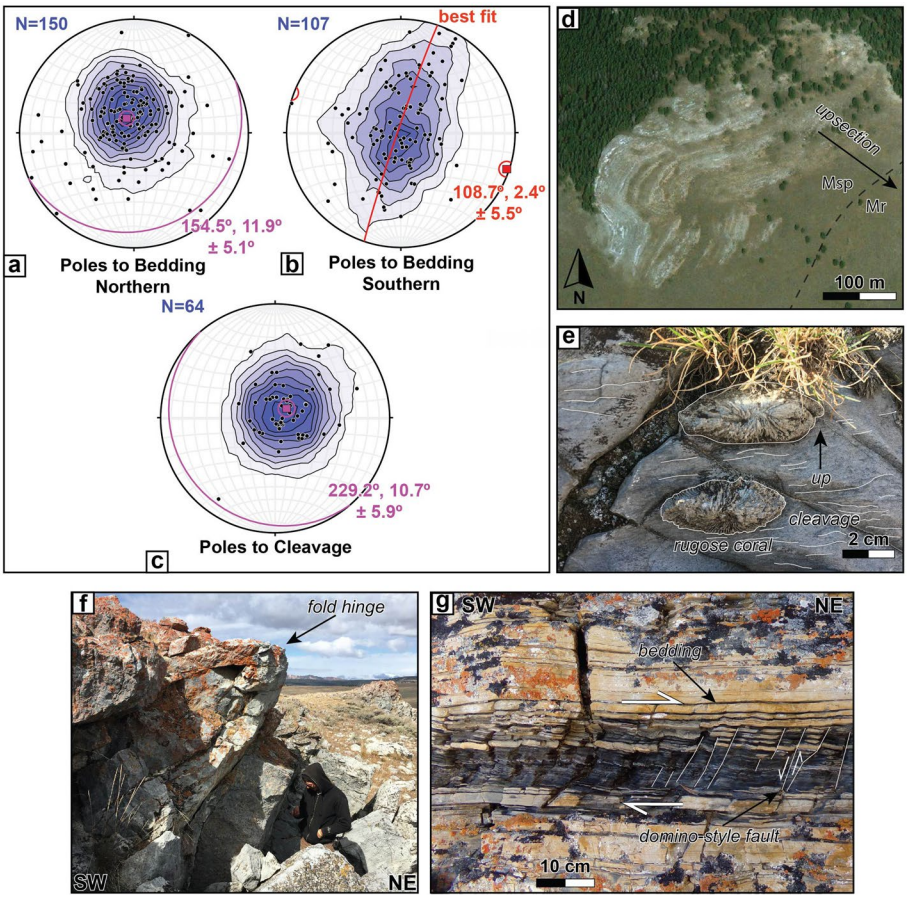

Figure 5. Deformation features of the sedimentary rock dip panel domain. Lower hemisphere stereographic projections showing: (a) Poles to bedding >1 km away from moderately dipping thrust faults. Mean vector and corresponding plane labeled. (b) Pi-plot of poles to bedding within 1 km of moderately dipping thrust faults. Cylindrical best fit and calculated fold hinge labeled. (c) Poles to cleavage. Mean vector and corresponding plane labeled. (d) Satellite photo showing folds in map view. (e) Outcrop photos of strained rugose coral in cross-section, (f) folded limestones near Grizzly Hill, and (g) bed-parallel shear in the Railroad Canyon Formation.

domain includes the non-mylonitized strata in the hanging walls of the basement-involved Radio Tower, Baby Joe Gulch, and Italian Gulch thrusts. The stratigraphy of the basement-rooted domain mostly defines the southern domain shown in Figure 4b.

Normal faults overprint all domains. Rarely observed brecciation within fault zones constrains fault dips of ~60°–70° toward the WSW and ENE. Offset of thrust faults across these normal faults constrains normal fault throw to <100 m. NNW-SSE striking normal faults apparently did not reactivate older deformation features resulting from horizontal shortening. These observations suggest that NNW-SSE striking normal faults post-date and are unrelated to deformation features accommodating horizontal shortening and will therefore not be discussed further.

4.2.1. Sedimentary Rock Dip Panel Domain

Within the gently southeasterly dipping section of the sedimentary rock dip panel domain, carbonate rocks of the Mississippian Scott Peak and Pennsylvanian Snaky Canyon formations are folded into tight folds with locally overturned limbs, northeast vergence, wavelengths of meters to tens of meters, and occasional small-offset thrusts in fold hinge zones (Figures 4 and 5). The observed folds lack continuity into adjacent units, indicating bedding-parallel detachment folding and some fault-propagation folding. Small, high-angle faults define angular, domino-style blocks with mm-scale down-to-the-SW normal offset (e.g.,

Goscombe et al., 2004) (Figure 5g), consistent with top-to-the-NE, bedding-parallel slip within the fine-grained Railroad Canyon Formation.

Poles to bedding within 1 km of the Radio Tower thrust ($N = 107$) define an east-southeast trending fold, with a calculated fold hinge plunging toward 109° at 2° (±6°) (Figure 5b). This distribution is 40% clustered and 30% girdled, suggesting complexities in addition to the mapped fold. Otherwise, poles to bedding planes ($N = 150$) are clustered ($P = 62\%$; $G = 2\%$) and define an average dip toward 155° at 12° (±5°) (Figure 5a).

At some localities, a pervasive, low-angle pressure solution cleavage was observed with poles to cleavage planes ($N = 64$) defining a clustered distribution ($P = 73\%$; $G = 8\%$) with a mean plane dipping toward 229° at 11° (±6°) (Figure 5c); this orientation is clearly not axial planar to upright detachment folds. Near Grizzly Hill, strained rugose corals ($N = 22$) have long axes that are parallel to cleavage, with a mean aspect ratio of 2.2 ± 0.5 (Figure 5e).

Cross-cutting relationships demonstrate that folding during bedding-parallel slip occurred before southeastward tilting within the sedimentary rock dip panel domain. The documented shallowly W-dipping pressure solution cleavage and associated subvertical shortening crosscuts folded bedding and is not associated with the hinge zones of folds, suggesting that cleavage formed after NE-directed folding. Tilting toward the southeast occurred after NE-directed folding. The tilted section continues ~10 km northwest of the study area, potentially related to the Peterson Creek thrust (Staatz et al., 1979).

4.2.2. Carbonate Mylonite Domain

4.2.2.1. General Description

Prior mapping by Lund (2018) and Lucchitta (1966) recognized fine-grained foliated carbonate rocks of inferred Mississippian age thrust over lesser deformed upper Paleozoic sedimentary rocks. These foliated carbonated rocks have a striking banded appearance, with calcite with siliceous interlayers on the mm-scale to cm-scale (Figure 6f). Segregation of dynamically recrystallized matrix grains (<20 μm) and deformed porphyroclasts define the foliation in thin section. In addition to mm-scale foliations, we document a previously unrecognized penetrative stretching lineation within these predominantly calcitic rocks (Figures 4, 5f, and 6f). The penetrative stretching lineation is defined by elongated aggregates of dynamically recrystallized grains, giving it a diffuse and streaky appearance on foliation surfaces (Figure 6f). Based on the pervasive foliation and abundant evidence of dynamic recrystallization, we interpret the foliated carbonates that define the Thompson Gulch (Lund, 2018) as carbonate mylonites (Bell & Etheridge, 1973; Fossen, 2016; White et al., 1980). Mylonite outcrops form klippen, with thicknesses ranging from 40 to 80 m based on good exposures in Thompson Gulch and Railroad Canyon (Figure 4). Exposures on ridges and in Railroad Canyon show a low-angle fault contact, at a low angle to bedding, leading us to classify both the Thompson Gulch and Railroad Canyon thrusts as thin-skinned.

Within the low-angle shear zones of both thrusts, particularly near Railroad Canyon, some siliceous interlayers have diffuse terminations parallel to the layering, suggesting that silicification of mm-scale to cm-scale interlayers was secondary and occurred during mylonitization. Tabular beds of matrix-supported calcareous breccia with sub-rounded clasts are often observed in fault contact with carbonate mylonite. In the immediate footwall of the Baby Joe Gulch thrust, between Thompson Gulch and Jakes Canyon (Figure 4), there is a recognizable tectonostratigraphy of calcareous breccia overlying tightly folded silicified black shales, which, in turn, overlie the carbonate mylonite. Elsewhere, calcareous breccia and silicified black shales are associated with the carbonate mylonite, but are not preserved in a consistent structural succession. Cliff-forming rocks in Jakes Canyon, previously mapped as chert of the Phosphoria Formation (Evans & Green, 2003; Lund, 2018), are completely silicified, matrix-supported breccias with banded clasts (Figure 8d) that we interpret as jasperoid (Lovering, 1962) overprinting carbonate mylonite.

4.2.2.2. Thompson Gulch Thrust

We refine the definition of the Thompson Gulch thrust by Lund (2018). Outcrops of carbonate mylonite define the shear zone, structurally above the sedimentary rock dip panel domain (Figure 4). The thrust cuts up-section in its footwall toward the east (Figure 4): in the western part of the map area near Jakes Canyon, the thrust occurs a few meters above the Devonian Jefferson Formation, within 10s of meters of the underlying Quartzite of Grizzly Hill; toward the east near Railroad Canyon, the thrust footwall consists

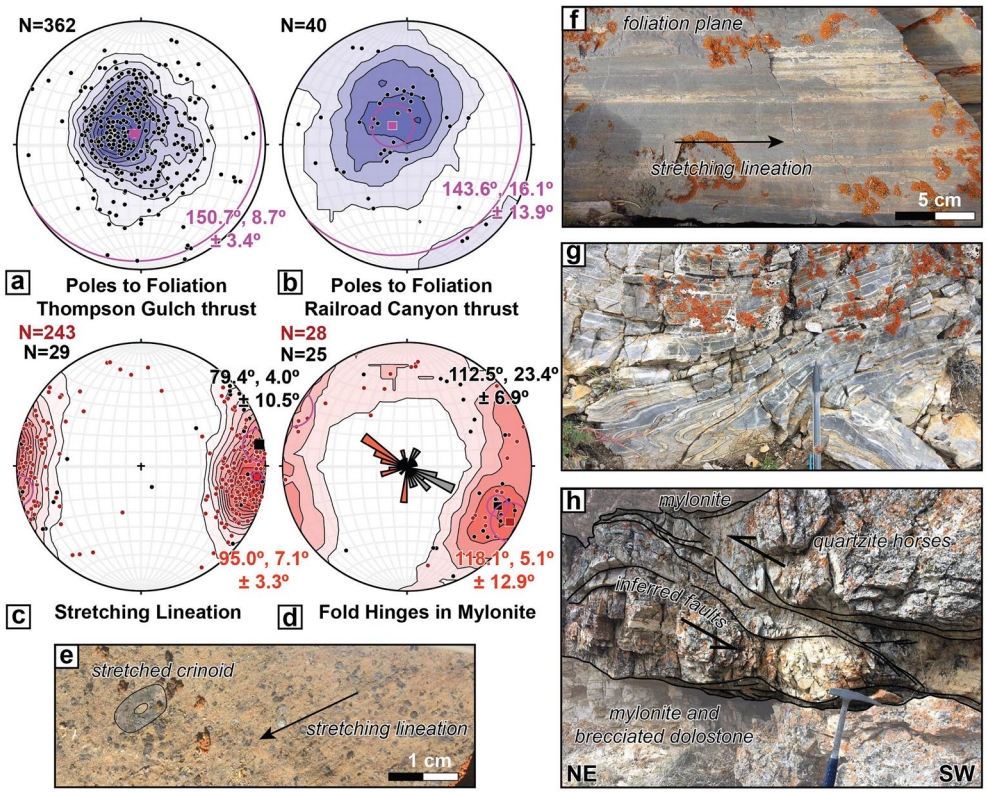

Figure 6. Deformation features of the carbonate mylonite domain. Lower hemisphere stereographic projections showing: poles to foliation of the (a) Thompson Gulch and (b) Railroad Canyon thrusts. Mean vector and corresponding plane labeled. (c) Stretching lineations with mean vectors of Thompson Gulch thrust data (red) and Railroad Canyon thrust data (black) labeled. (d) Fold hinges within mylonite with mean vectors labeled for post-mylonite (black) and syn-mylonite (red) folds. Inset rose diagram with 10° bins shows distribution of trends. Outcrop photos of (e) stretched crinoid ossicle as viewed in plan view, (f) typical carbonate mylonite as viewed in plan view, (g) recumbent similar folds within otherwise parallel foliation as viewed in cross-section, and (h) quartzite horses between mylonite and brecciated dolostone as viewed in cross-section.

of the Pennsylvanian Snaky Canyon Formation. Below the lowest exposure of the mylonite in the western part of the map area, 1–2 m thick horses of quartzite are thrust-bounded and merge upward into the superjacent mylonite (Figure 6h); slickenline orientations on faults that bound the margins of the horses within the quartzite are indistinguishable from the orientations of stretching lineations in the overlying carbonate mylonite.

Plotted poles to foliation planes for the mylonite of the Thompson Gulch thrust ($N = 362$) show a clustered distribution ($P = 56\%$; $G = 8\%$), with a mean plane dipping toward 151° at 9° (±3°) (Figure 6a). The mylonite contains tight, recumbent folds in close proximity to planar foliations (Figure 6g). Rare shear bands are interpreted as C-C′ fabrics. Boudins, minor brittle normal faults, and veins are uncommon (labeled red localities 1, 2 in Figure 4) and overprint earlier mylonites. Stretching lineations ($N = 243$) show a clustered distribution ($P = 72\%$; $G = 4\%$) and define a mean vector of 095°, 7° (±3°) (red dots, Figure 6c). Crinoid ossicles on foliation planes are elongate parallel to the stretching lineation (Figure 6g), with a mean aspect ratio of 1.7 ± 0.4 ($N = 11$).

In thin section, the mylonite of the Thompson Gulch thrust is mostly fine-grained (<20 μm grain diameters in matrix grains) with a subhorizontal shape-preferred orientation, and only rare asymmetric clasts indicative of noncoaxial strain. Coarse (>100 μm) calcite grains are characteristically twinned with tabular and sometimes curved morphologies (Figure 7d). Oriented thin sections (5, 6, 7, 9 in Figure 4) display σ-clasts, strain fringes, offset veins, and C-C' shears that give a consistent top-to-the-E sense of slip (Figures 7c–7e). An outcrop along the western side of Thompson Gulch (Figure 7) clearly shows C-C′ shear structures with

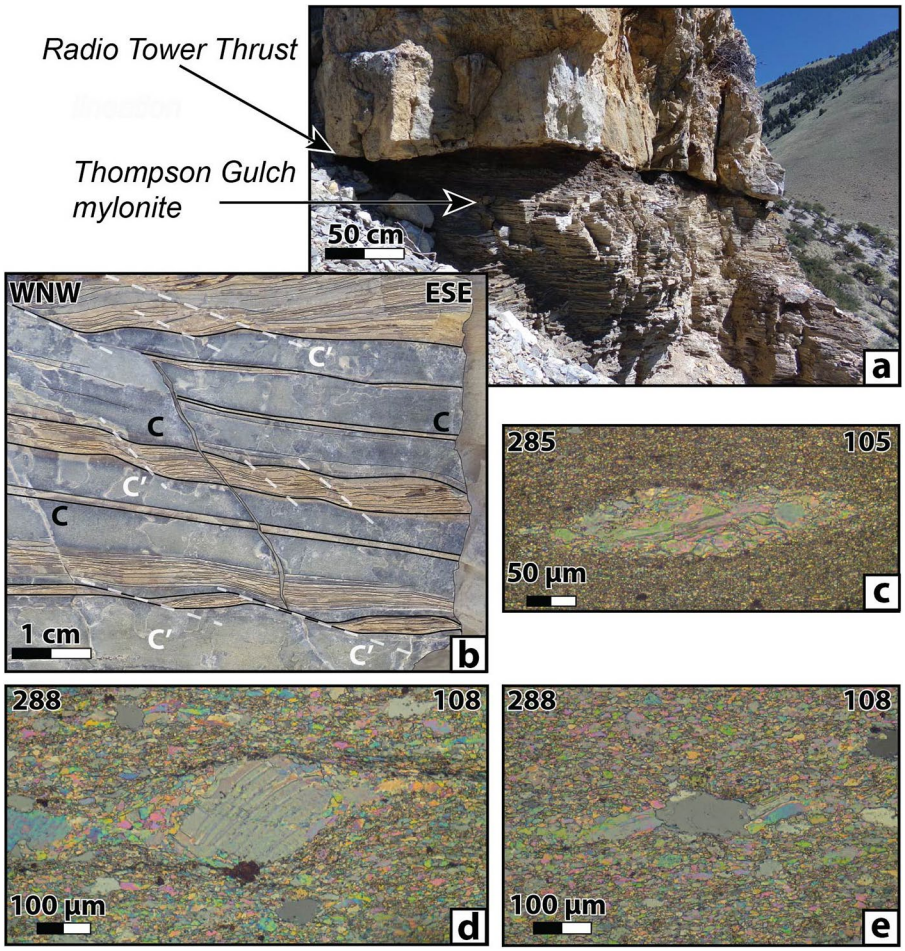

Figure 7. (a) Outcrop photos showing fault contact of Radio Tower thrust and underlying Thompson Gulch mylonite (labeled red locality 3 in Figure 4), and (b) top-to-the-ESE C and C′ shear fabrics within the Thompson Gulch mylonite. Oriented thin section photomicrographs showing (c) σ-clast (location 3 in Figure 4, (d and e) σ-clast and calcite fibers in strain fringes around quartz grain (labeled red locality 4 in Figure 4) all with a top-to-the-ESE sense of shear.

an apparent top-to-the-ESE sense of shear within the shear zone of the Thompson Gulch thrust. At this location, the mylonite of the Thompson Gulch thrust is in sharp contact with an overlying ~1 m thick, planar, matrix-supported breccia that defines a brittle fault zone interpreted as the Radio Tower thrust.

Folds within the mylonite are split into two categories: syn-mylonitic and post-mylonitic. Syn-mylonitic folds are commonly non-cylindrical, tight to isoclinal, similar folds with wavelengths from ~10 to 20 cm (Figure 6f); sheath folds were also observed. Post-mylonitic folds are commonly cylindrical, tight to open, parallel folds with m-scale wavelengths; tight fold hinges are often brecciated. The orientations of both fold sets are very scattered, with a mean fold hinge of 118°, 5° (±13°) for syn-mylonitic folds and 113°, 23° (±7°) for post-mylonitic folds (Figure 6d). Both sets of folds have gently plunging hinges, resulting in an overall girdled distribution of plotted lines ($P = 28\%$; $G = 47\%$). Post-mylonitic folds are more often highly oblique to the stretching lineation. Near Railroad Canyon, post-mylonitic folds of the outcrop-scale to km-scale are NE-SW-trending, in the footwall of the Italian Gulch thrust (red localities 1, 2 in Figure 4).

The interlayered carbonate, silicified shales, and local dolostone associated with the mylonite, as well as stretched crinoids in the shear zone, are consistent with a protolith within the lower half of the Paleozoic stratigraphy of the sedimentary rock dip panel (northern domain in Figure 4b). Results from mapping and structural analysis suggest overall eastward thrusting of the Thompson Gulch thrust hanging wall. Shallowly W-dipping pressure solution cleavage and sub-vertical flattening of rugose corals in the footwall of the Thompson Gulch thrust (sedimentary rock dip panel domain) are interpreted to have accommodated

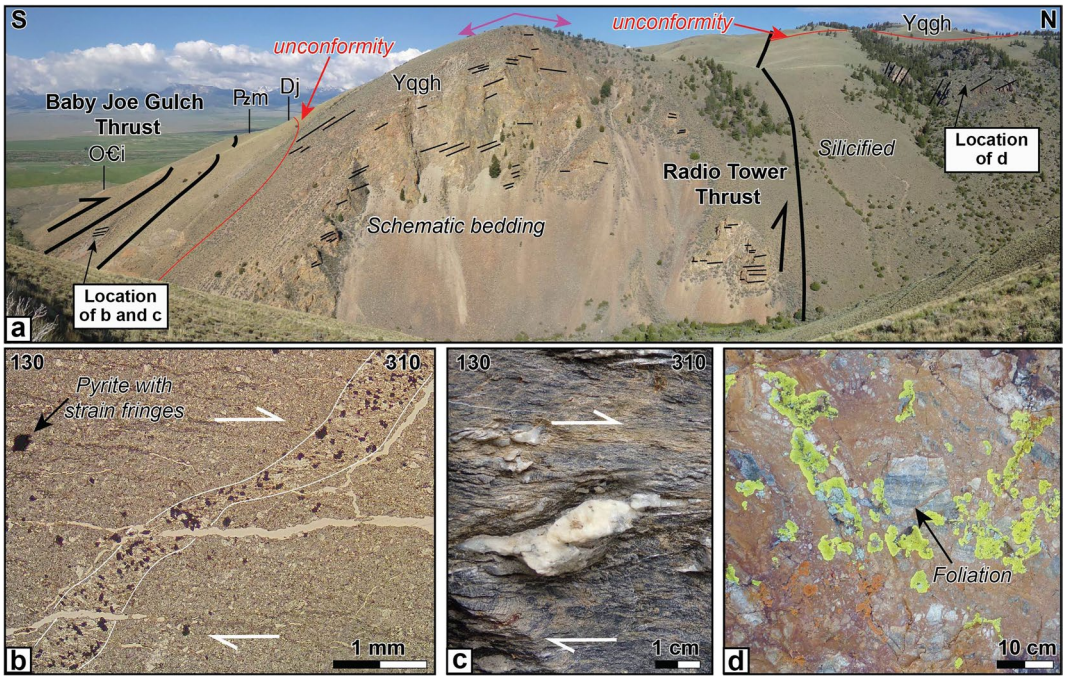

Figure 8. Field relationships and kinematics from the western side of Jakes Canyon (red locality 7 in Figure 4). (a) Thrust fault contacts marked in bold black lines, with fine black lines defining bedding orientation and an overall anticlinal structure (purple arrows). Red lines show the intra-Devonian Lemhi arch unconformity. *Note*: the Baby Joe Gulch thrust does truncate bedding at a low angle. (b) Oriented thin section from the immediate footwall of the Baby Joe Gulch thrust showing vein with a top-to-the-NW sense of offset. Outcrop photos of (c) σ-clast with a top-to-the-NW sense of shear and (d) silicified breccia with relict foliation in clasts.

shear zone-normal flattening during thrusting, or alternatively may have been rotated during progressive noncoaxial shear as a result of diffuse deformation in the footwall of the Thompson Gulch thrust. The section was tilted toward the southeast either before or after thrusting. The shear zone of the Thompson Gulch thrust is a low-angle feature that spans more than 10 km (in the direction of transport) but involves only the thin portion of the stratigraphic section (<800 m) that contains silty and shaley intervals, demonstrating a correspondence with weak lithologic units. We therefore classify the Thompson Gulch thrust as thin-skinned. The Thompson Gulch thrust is truncated and folded by—and therefore older than—thrusts of the basement-rooted domain.

4.2.2.3. Railroad Canyon Thrust

In the southern part of the map area, carbonate mylonite indistinguishable from that of the Thompson Gulch thrust crops out in a different structural position in the hanging walls of the Italian Gulch, and Baby Joe Gulch thrusts. Between Jakes Canyon and Railroad Canyon, carbonate mylonite overlies the Beaverhead pluton and Kinnikinic Quartzite (red locality 8 in Figures 4 and 9d). Exposures in Railroad Canyon show a hanging-wall flat of the Saturday Mountain Formation above the mylonite (red locality 1 in Figure 4). We assign the new name Railroad Canyon thrust to mylonites at this position.

Stretching lineations of the Railroad Canyon thrust (N = 29) have a clustered distribution (P = 64%; G = 14%) and define a mean vector of 79°, 4° (±11°) (black dots, Figure 6c). Plotted poles to foliation planes (N = 40) show a loosely clustered distribution (P = 42%; G = 10%), with a mean vector defining a pole to a plane that dips toward 144° at 16° (±14°) (Figure 6b).

The overall similarities in lithology, geometry, and kinematics of the Railroad Canyon and Thompson Gulch thrust mylonites suggest they formed as part of the same sequence of deformation. We make a distinction between the two based on differing footwall stratigraphy. Unlike the Thompson Gulch thrust, the hanging wall geometry is well constrained near Railroad Canyon, where a hanging wall flat overlies the shear zone.

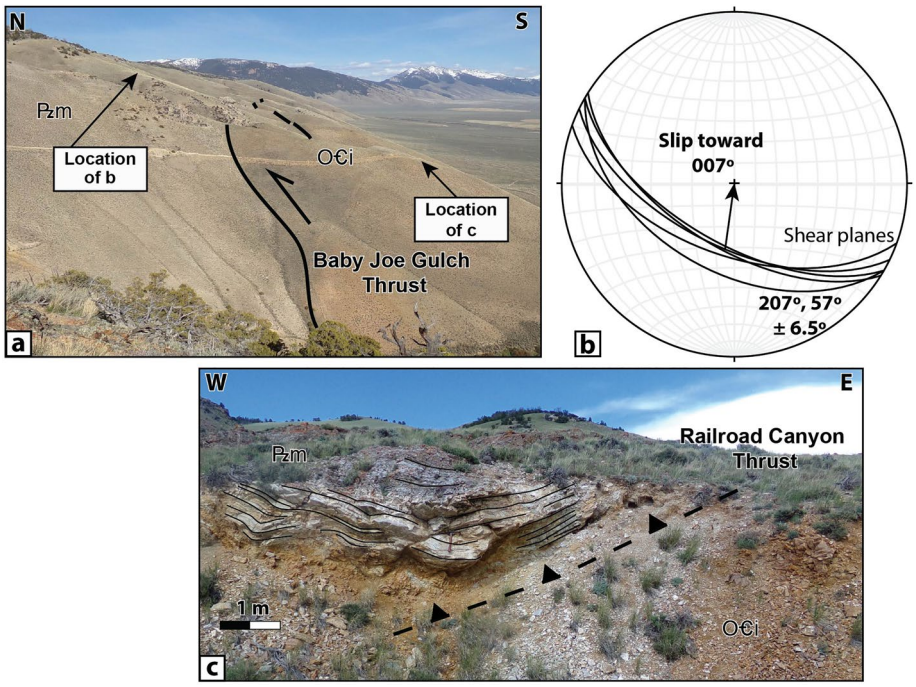

Figure 9. Field relationships from the eastern side of Jakes Canyon (red locality 8 in Figure 4). (a) Along-strike view of the Baby Joe Gulch thrust, fault contact shown in black line and arrow on hanging wall. (b) Lower hemisphere stereographic projection of shear planes (black lines) with arrow showing slip direction of the hanging wall. (c) Outcrop photo showing low-angle fault contact of the Railroad Canyon thrust. Black lines highlight foliation of the hanging wall.

We therefore classify the Railroad Canyon thrust as thin-skinned. Like the Thompson Gulch thrust, the Railroad Canyon thrust was offset by—and therefore older than—thrusts of the basement-rooted domain.

4.2.3. Basement-Rooted Domain

4.2.3.1. General Description

The hanging walls of the moderately to steeply dipping Baby Joe Gulch (Lund, 2018), Radio Tower, and Italian Gulch thrusts define the basement-rooted domain (Figures 4 and 8). These thrusts cut across bedded quartzites and plutonic rocks with no apparent relation to primary layering, suggesting that these rocks behaved as mechanical basement. We therefore categorize the Radio Tower, Baby Joe Gulch, and Italian Gulch thrusts as thick-skinned thrusts.

4.2.3.2. Radio Tower Gulch Thrust

A steeply (50°–70°) S-dipping fault in Jakes Canyon, named here the Radio Tower Gulch thrust, juxtaposed the Mesoproterozoic Quartzite of Grizzly Hill over partly mylonitized and silicified younger footwall rocks that we tentatively assign to the Devonian Jefferson through Mississippian Middle Canyon formations (Figures 8a and 8d). The intra-Devonian Lemhi arch unconformity shows ~1 km of apparent sinistral separation across the E-W Radio Tower thrust (Figure 4). Hanging wall and footwall strata are folded by ESE-WNW-trending folds. East of Jakes Canyon, apparent stratigraphic separations were used to continue the uncertain trace of the fault to Thompson Gulch, where a moderately W-dipping thrust is well-exposed (Figure 7a). The difference in dip along the fault plane requires folding or a complex fault geometry. The Radio Tower thrust clearly cuts the Thompson Gulch thrust in several locations and is therefore younger.

4.2.3.3. Italian Gulch Thrust

East of Thompson Gulch, the Ordovician Kinnikinic Quartzite and the structurally overlying mylonite of the Railroad Canyon thrust were thrust upon a footwall of mylonite of the Thompson Gulch thrust; we name this fault the Italian Gulch thrust. Unlike its footwall, the hanging wall of the Italian Gulch thrust

carried the sub-Ordovician Lemhi arch unconformity and Ordovician to Devonian strata. Where best constrained, west of Italian Gulch, the fault dips toward the south or southeast at 30°–50°. Both ENE-WSW-trending and ESE-WNW-trending folds occur within the hanging wall and footwall of the Italian Gulch thrust. The Italian Gulch thrust clearly cuts the Thompson Gulch and likely the Railroad Canyon thrusts and is therefore younger. The presence of the sub-Ordovician Lemhi arch unconformity and overlying Ordovician and Silurian rocks in the hanging wall of the Italian Gulch thrust indicates a striking difference in pre-thrusting stratigraphy.

4.2.3.4. Baby Joe Gulch Thrust

The structurally highest thrust in the study area is the Baby Joe Gulch thrust, named by Lund (2018). Its trace is well-constrained from Jakes Canyon to Italian Gulch, where it cuts all other thrusts (Figure 4). Unlike other mapped thrust faults that are either inferred with poorly constrained orientations (Italian Gulch thrust) or vary in orientation, possibly due to folding (Thompson Gulch, Railroad Canyon, and Radio Tower thrust) the Baby Joe Gulch is remarkably planar along most of its trace. The precisely mapped contact allows us to tightly constrain the orientation of the fault plane. Three-point problems define the fault that dips toward 198° at 38° (±9°), roughly parallel to a weakly developed solid-state foliation within the Beaverhead pluton (Figure 4). Across Italian Gulch, the trace of the Baby Joe Gulch thrust and foliation within the Beaverhead pluton transition from SSW-dipping to the west to SE-dipping toward the east. The trace of the Baby Joe Gulch thrust either intersects or merges with the trace of the Italian Gulch thrust east of Italian Gulch. The apparent dip of the Baby Joe Gulch thrust becomes less similar to that of the Italian Gulch thrust as you near their intersection, making it more likely that the Baby Joe Gulch thrust is truncated by the Italian Gulch thrust.

In the immediate footwall of the Baby Joe Gulch thrust on the eastern side of Jakes Canyon, post-mylonitic asymmetric kink bands ($N = 5$) define a mean shear plane dipping toward 207° at 57° (±7°) (Figure 9b), with sigmoidal calcite veins suggesting a thrust sense of slip toward 7°. On the western side of Jakes Canyon (7 in Figure 4), post-mylonitic shear zones have ~10 cm spacing and define a mean plane ($N = 4$) dipping toward 140° at 30° (±11°), with a top-to-the-NW sense of shear at the outcrop-section and thin-section scale (Figures 8b and 8c). Shear zones cut a low-angle crenulation cleavage, and both the crenulation cleavage and veins within the shear zones are folded. We are not confident that these kinematics are representative of the shortening direction of the Baby Joe Gulch thrust. We include these observations because they suggest different shortening directions for the Thompson Gulch and Baby Joe Gulch thrusts.

The Baby Joe Gulch thrust is apparently the youngest thrust in the study area: it cut the approximately flat-lying mylonites of the Thompson Gulch and Railroad Canyon thrusts as well as the steeply dipping Radio Tower and Italian Gulch thrusts. Its approximately northeast or northwestward displacement direction is highly oblique to that of the older Thompson Gulch thrust. Like the Italian Gulch thrust, the Baby Joe Gulch thrust carried a substantially different stack of rocks in its hanging wall. In the hanging walls of these thrusts, ~250 m of fossiliferous Ordovician to Devonian dolostones and an additional ~150 m of Ordovician sandstone rest unconformably on the Cambro-Ordovician Beaverhead pluton. These rocks are completely absent in the corresponding footwalls, where the exceptionally thin (~50 m) laminated dolostone of the Devonian Jefferson Formation (upper) rests directly on Mesoproterozoic quartzite. Restoration of the Italian Gulch and Baby Joe Gulch thrusts therefore requires pre-Devonian normal faults. These results suggest that "late-stage," out-of-sequence thrusting associated with the Baby Joe Gulch thrust cut the mechanical basement of the Lemhi arch in a thick-skinned style, and likely reactivated older normal faults.

4.3. Summary of Deformation Events

Progressive thin-skinned to thick-skinned thrusting of the study area is summarized in three deformation events (Figure 10). In the sedimentary rock dip panel domain, a low-angle pressure solution cleavage overprints NE-verging detachment folds. The cleavage parallels foliation within the neighboring shear zone of the Thompson Gulch thrust. This relationship constrains the early phases of deformation. First, laterally continuous sedimentary cover rocks above the intra-Devonian Lemhi arch unconformity underwent NE-SW layer-parallel shortening (Figure 10a). Second, sedimentary cover rocks were transported toward the east along a subhorizontal thin-skinned Thompson Gulch thrust (Figure 10b). Like the Thompson

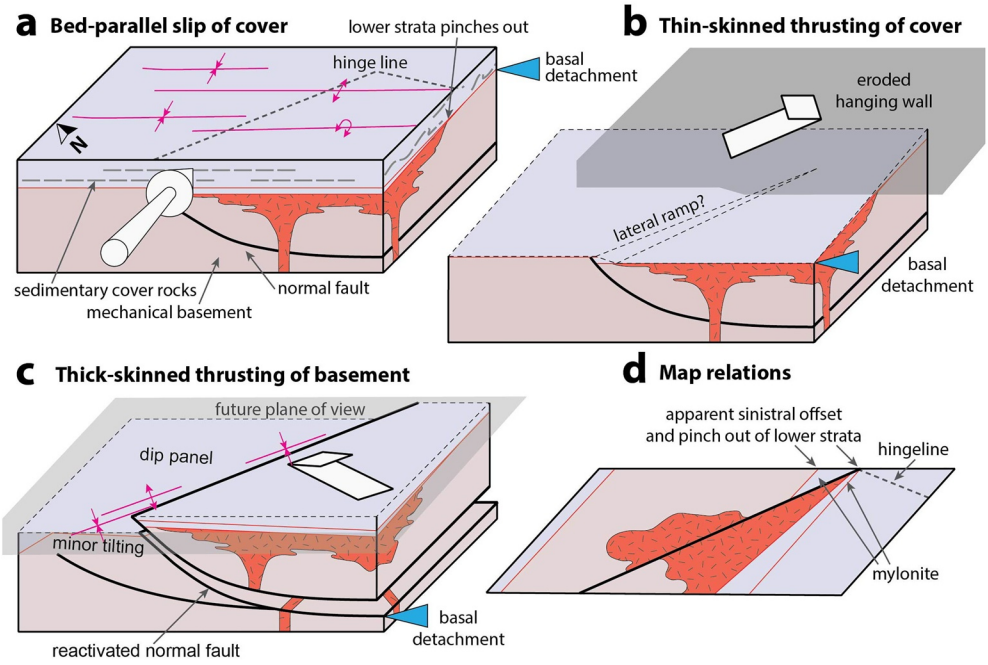

Figure 10. Simplified block diagrams showing the hypothesized series of deformation events and inferred basal detachment (a–c) used to explain the observed map relations (d). Lemhi arch unconformities shown in red. Pink fold symbols show orientation of active folds.

Gulch thrust, the Railroad Canyon thrust also contains calcareous mylonites and has a parallel, penetrative stretching lineation, suggesting similar deformation conditions and kinematics, but involving rocks at a different stratigraphic level between the sub-Ordovician and intra-Devonian Lemhi arch unconformities that pinch out to the north and east. A lateral ramp across the intra-Devonian Lemhi arch unconformity (Figure 10b) may directly link the Thompson Gulch and Railroad Canyon thrusts, or they may be separate faults that were both active before thick-skinned thrusting. The Thompson Gulch and Railroad Canyon thrusts are truncated by the Radio Tower, Italian Gulch, and Baby Joe Thrusts, constraining the relative timing of deformation. Finally, the basement and cover rocks were tilted to the southeast by 5°–15° (Figure 10c) during activation of a deeper basal detachment horizon below the basement-cover contact, which must be linked to a thick-skinned thrust fault northwest of the current study area. Basement and cover rocks of the tilted sections were shortened, oblique to the previous shortening direction, along the thick-skinned Radio Tower, Italian Gulch, and Baby Joe Gulch thrusts (Figure 10c). The restored stratigraphic relationships of the Lemhi arch unconformities and the striking differences in pre-thrusting stratigraphy suggest thrust reactivation of a pre-Devonian normal fault, which was oblique to the regional shortening direction. These deformation events explain the apparent offsets and crosscutting relationships observed in the map relations (Figure 10d).

5. Discussion

5.1. Transition in Structural Style Over a Basement High

The study area exposes not only contrasting structural styles near the base of a thin-skinned thrust belt, but also major stratigraphic changes that define a regional basement high in the western North American passive margin. The transition from thin-skinned to thick-skinned thrusting documented here coincides with an exceptionally thin stratigraphic section overlying the basement high (Figure 3). The Jefferson and McGowan Creek formations mark the basement/cover contact and dramatically thicken toward the interior of the fold-thrust belt (Figure 3), from a local thickness of ~80 m to >2 km in the Lost River Range ~75 km toward the southwest (Grader & Dehler, 1999; Grader et al., 2017). The total preserved thickness of the stratigraphic section is locally 1.8 km, comparable in thickness to correlative sections throughout

the Beaverhead and Tendoy mountains toward the foreland (Peterson, 1981; Rose, 1976; Scholten, 1957), but much thinner than the ~3–3.5 km in the Lemhi Range, and ~4 km in the Lost River Range (Ruppel & Lopez, 1988). Upper units (above the intra-Devonian Lemhi arch unconformity) are conformable and laterally continuous over the ~250 km width of the Idaho-Montana fold-thrust belt. Lower units (between the young and old unconformities) completely pinch out over the Lemhi arch basement high, becoming absent in the northern part of the study area and toward the front of the fold-thrust belt. The study area therefore marks a pronounced hinge line, where lower stratigraphic units thin drastically and/or pinch out near the regional basement high. As a result, regional stratigraphic weak layers are thinner, shallower, or absent altogether where the transition from thin-skinned to thick-skinned thrusting occurs.

From the range of rheologies documented by deformation features, we can constrain approximate deformation temperatures and depths, thereby refining the relationship between the preexisting stratigraphy and the resulting fold-thrust belt. Deformation features in quartzose and dolomitic rocks of the study area are entirely brittle, whereas calcitic rocks record plastic deformation. Widespread dynamic recrystallization was observed, where significant grain size reduction resulted in grain sizes generally <20 μm, as is expected for a carbonate rock undergoing deformation at low temperatures (~150°C–300°C; e.g., Burkhard, 1990; DeBresser et al., 2002). The observed tabular, thick, and sometimes curved calcite twins (Figure 7d) are characteristic of Type II and Type III twins (Burkhard, 1993; Ferrill et al., 2004), suggesting a rough temperature range of 200°C–250°C. This is in agreement with an independent maximum temperature estimate of 190°C–300°C (Dembicki, 2016) obtained from a conodont color alteration index of "4" for a sample of Mississippian rocks (Perry et al., 1983) collected along Railroad Canyon ~5 km north of the study area. Assuming a 20°C surface temperature and geothermal gradient of 25–30°C/km, temperatures of 200°C–250°C suggest a depth of deformation of 6–9 km. The study area thus offers the unique opportunity to directly observe the underlying mechanical basement, within the lower structural levels of a classic thin-skinned thrust belt nearly 50 km from the frontal thrust. This fortuitous view allows for us to discuss how structural style varies across-strike, along-strike, and with depth.

Given that the inferred range of protoliths of the carbonate mylonite is Ordovician (Saturday Mountain Formation) to Mississippian (Middle Canyon Formation) in age, we reconstructed the stratigraphic burial depths of these rocks using results from the current study area (for Ordovician to Pennsylvanian rocks) coupled with regional constraints (Skipp, 1988) where the overlying rocks were removed in the study area due to erosion (Triassic to Cretaceous rocks). The reconstructed overlying thickness of rocks ranges from ~3.2 to 3.5 km. Assuming a 25°C/km geothermal gradient, 2.5–6 km of additional strata must have been present above the basal detachment of the study area, to achieve temperatures between 200°C and 250°C. Thickening related to distributed horizontal shortening may simply account for most of the missing overburden. Assuming plane strain, a rough area-balanced shortening estimate requires ~42%–65% horizontal shortening above the carbonate mylonite to achieve 2.5–6 km of vertical thickening above the basal detachment. This shortening magnitude is comparable with estimates for other thin-skinned portions of the Cordillera (e.g., DeCelles & Coogan, 2006; Mitra, 1994). In the neighboring Lemhi Range, km-scale recumbent folds accommodate similar magnitudes of shortening at comparable stratigraphic levels (Beutner, 1968; Hait, 1965). Burial before slip along the Thompson Gulch thrust was most likely due to distributed folding and not an overlying thrust sheet, given the widespread folding in the region (Beutner, 1968; Hait, 1965; Messina, 1993) and general absence of major thrusts to the west of the study area (Figure 2). Substantial subvertical shortening associated with the shear zones of the thin-skinned thrusts of the study area likely reflects local flattening in the shear zone, and not distributed ductile thinning related to large-scale thickening of the crust (cf., Long & Kohn, 2020). Regional-scale horizontal shortening was accommodated by a combination of folding, thrusting, and localized ductile shearing, all of which involved only the sedimentary cover rocks above the basement high of the Lemhi arch.

Structurally below the sedimentary rock cover succession, the quartzose mechanical basement was horizontally shortened by later thick-skinned thrusting under brittle conditions. The apparent sinistral separation across the S-dipping Radio Tower and Baby Joe Gulch thrusts (Figure 4) can be explained simply by ~N-directed thrusting across a dip panel with an apparent dip toward the east (Figures 10c and 10d). Following this model and using the intra-Devonian Lemhi arch unconformity as a piercing point, we estimate that ~2 km of total horizontal shortening of the mechanical basement occurred on the Radio Tower and

Baby Joe Gulch thrusts. Sinistral slip along these faults is also possible, but would require >7 km of E-W slip, which is less likely given the observed kinematics of the Baby Joe Gulch thrust. Estimated shortening magnitudes for the Hawley Creek thrust range from a minimum ~1 km (Skipp, 1988) to upwards of ~3 km of horizontal shortening as suggested by the juxtaposition of Ordovician and Triassic strata (e.g., Lucchitta, 1966). Late-stage thick-skinned thrusting was therefore relatively minor and likely oblique compared to earlier thin-skinned thrusting. Given our small sample size, the kinematic indicators we report for the Baby Joe Gulch thrust may not be representative of the overall slip direction. Though the shortening direction is poorly constrained, reactivation of a pre-Devonian normal fault is suggested by the juxtaposition of drastically different Ordovician to Devonian stratigraphy across the fault. Detailed sequence stratigraphic studies of the Devonian Jefferson Formation support this interpretation (Grader et al., 2017). The oblique orientation of the inherited normal fault to the regional shortening direction may have controlled the apparent change in the local shortening direction. This interpretation is consistent with previous studies that document local strain refractions near thick-skinned structures that are oblique to the regional shortening direction, consistent with reactivation of pre-existing basement weaknesses (e.g., Erslev & Koenig, 2009; Kley & Monaldi, 2002; Marshak et al., 2000; Neely & Erslev, 2009; Weil & Yonkee, 2012; Weil, Yonkee, & Schultz, 2016).

5.2. Age of Deformation

The documented transition in structural style from early thin-skinned to late thick-skinned deformation is well-constrained by the mapped crosscutting relationships. However, assigning absolute ages to these phases of deformation is more difficult due to the lack of dateable syn-deformational rocks. In neighboring quadrangles, folded and cleaved rocks in the deformed footwall of the Thompson Gulch thrust include rocks as young as Triassic (e.g., Lucchitta, 1966) and are overlapped by unfolded volcanic and sedimentary rocks of lower to middle Eocene age (Lonn et al., 2019; VanDenburg, 1997). Additional age constraints come from recent detrital zircon provenance studies within synorogenic Beaverhead Group foreland basin rocks of southwestern Montana (Garber et al., 2020), which record arrival of distinctive ~500 Ma Beaverhead pluton (Evans & Zartman, 1988; Link et al., 2017; Lund et al., 2010) detrital zircons. Given that outcrops of the Beaverhead pluton are confined almost entirely to the hanging walls of the Poison Creek-Baby Joe Gulch-Hawley Creek thrust system (e.g., Link et al., 2017), the ~500 Ma zircons are a unique population that are present only in sediment derived from the late phase of thick-skinned deformation. The first occurrence of ~500 Ma zircons derived from the Beaverhead pluton occurs within strata with a maximum depositional age of ~67 Ma (Garber et al., 2020), which is very similar to zircon (U-Th)/He ages from the hanging wall of the Poison Creek thrust, which give weighted mean cooling ages of 68.4 ± 0.9 Ma ($N = 6$) and 56.8 ± 0.7 Ma ($N = 5$) (Hansen & Pearson, 2016). We therefore interpret that the early phase of thin-skinned deformation predates the ~68 Ma phase of thick-skinned deformation.

5.3. Double-Decker Thin-Skinned to Thick-Skinned Fold-Thrust Belt

The deformation events of the study area (Figure 10) highlight slip along increasingly deeper basal detachments with progressive deformation, resulting in a shift from thin-skinned to thick-skinned deformation, more than 50 km behind the leading edge of the thin-skinned wedge. This interpretation is consistent with the regional trend (Figure 2) of an upper thin-skinned system that is deformed by a lower thick-skinned system. Thus, as described by some prior workers, the Sevier belt and Laramide province of the Idaho-Montana fold-thrust belt cannot be divided by a single line on the map (Kulik & Schmidt, 1988; O'Neill et al., 1990). Instead, the boundary between thin-skinned and thick-skinned domains is low-angle: early, thin-skinned thrusting at high structural levels overlapped in timing with and was later overprinted by thick-skinned thrusting at lower levels. Taiwan and the Zagros are other notable examples that were originally interpreted as thin-skinned belts (Davis & Engelder, 1985; McQuarrie, 2004; Namson, 1981; Suppe & Namson, 1979), but are now interpreted to have deeper thick-skinned thrusts that disrupt the overlying thin-skinned detachment horizons (Allen et al., 2013; Hung et al., 1999; Lacombe & Bellahsen, 2016; Lacombe & Mouthereau, 2002; Le Garzic et al., 2019; Molinaro et al., 2005; Mouthereau, Lacombe, & Meyer, 2006; Mouthereau, Lacombe, & Vergés, 2012; Mouthereau et al., 2007; Sherkati et al., 2006; Yang et al., 2001).

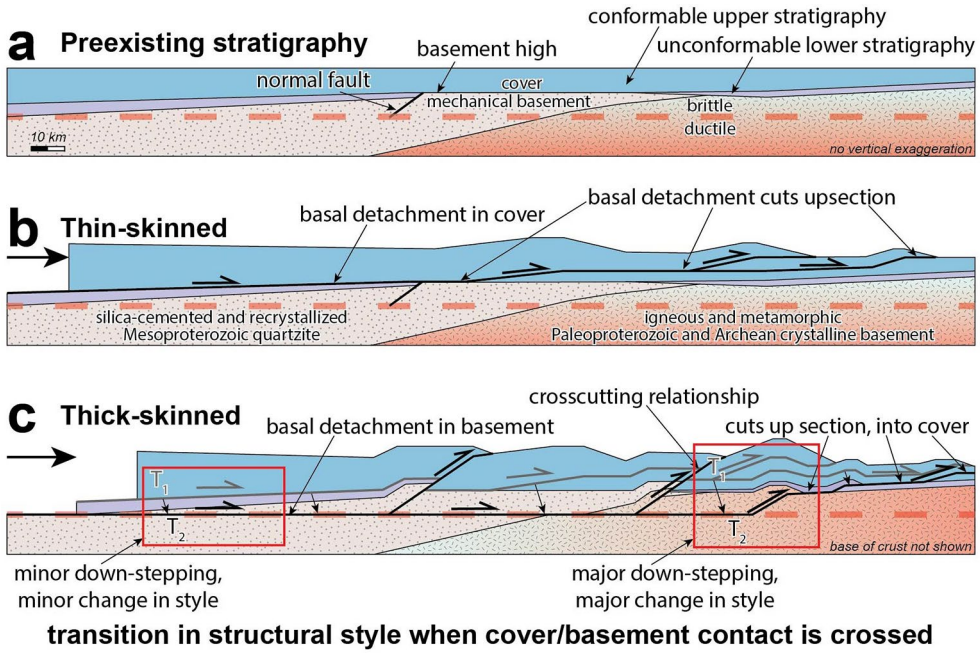

Figure 11. Schematic cross-sections illustrating the double-decker model: (a) initial undeformed state, (b) early thin-skinned thrusting, and (c) later thick-skinned thrusting.

Despite the clear value of critical taper theory, the shift toward more hybrid thin-skinned and thick-skinned models challenges one significant assumption of the model: that a pre-thrusting throughgoing basal detachment horizon is utilized throughout deformation (e.g., Buiter, 2012; Davis et al., 1983). It has long been recognized that thick-skinned belts often occur within thin packages of sedimentary cover rocks (Allmendinger et al., 1983; Fitz-Díaz et al., 2018; Kley et al., 1999; Pearson et al., 2013; McGroder et al., 2015; S. A. Williams et al., 2020) and that thin-skinned belts are wider where sedimentary cover rocks are thicker (Marshak, 2004; Yonkee & Weil, 2010). Because the critical taper angle depends on intrinsic mechanical properties, the width and height of a thin-skinned wedge are limited by the thickness of sedimentary cover rocks (e.g., Boyer, 1995). If sedimentary cover rocks are very thin, such as demonstrated for the Lemhi arch (Figure 3), activation of a deeper basal detachment horizon within the mechanical basement may be required to thicken the wedge and balance the stress state before more horizontal shortening can be accommodated. If the basement-cover unconformity is very steep, as inferred for the Lemhi arch (Figure 3), it may be easier to reactivate preexisting weaknesses at deeper crustal levels than to short-cut the basement high and create a basement-involved duplex (e.g., Boyer & Elliott, 1982; Yonkee, 1992). Furthermore, if weak, viscous detachments deep in the crust are activated, then the wedge taper angle may be significantly reduced, promoting the propagation of the wedge after minimal internal shortening (Ruh et al., 2012; C. A. Williams et al., 1994). Regardless, when a thin-skinned wedge is too thin and/or the basal detachment is too strong to achieve critical taper by shortening internally and increasing the surface slope, then activation of a deeper detachment horizon provides a way to achieve critical taper by increasing the basal slope. In thin stratigraphic wedges, this may result in a transition from thin-skinned to thick-skinned structural style.

The results of this study add to the growing list of observations that suggest a regionally continuous thin-skinned fold-thrust belt within the Idaho-Montana fold-thrust belt that was later dissected by a deeper thick-skinned thrust system. Our preferred interpretation—that the Thompson Gulch thrust is the transient basal detachment of a former thin-skinned fold-thrust belt—is consistent with the examples shown in Figure 2 and described earlier in the text, which suggests regional continuity of deformation above the Lemhi arch when slip is restored on deeper crosscutting structures.

Based on the results of this study and the documented variations in structural style with depth across the Idaho-Montana fold-thrust belt, we propose a double-decker model (Figure 11) that more accurately describes the geometry of structural style domains and offers testable predictions for continental fold-thrust

belts elsewhere (e.g., Taiwan and Zagros, Lacombe & Bellahsen, 2016). Thin stratigraphy, such as over a basement high (Figures 11a), promotes thick-skinned thrusting when the stratigraphy is too thin to fit the required critically tapered wedge. Initial thin-skinned thrusting is widespread when the growing orogenic wedge fits entirely above the basement/cover contact (Figures 11b). In the Idaho-Montana fold-thrust belt, early thin-skinned thrusting from the Lost River Range to the Blacktail Mountains is evident from widely distributed NE-verging detachment folds that are ubiquitous above the intra-Devonian Lemhi arch unconformity (e.g., Anastasio et al., 1997; Lonn et al., 2000; Perry & Sando, 1982).

With continued horizontal shortening, the thin-skinned wedge grows, requiring activation of a deeper basal detachment near the front of the orogenic wedge. When a basement high is present, the basal detachment must advance into the underlying basement high, promoting a transition from thin-skinned to thick-skinned thrusting (Figures 11c). The widespread occurrence of mechanical basement and the presence of both thin-skinned and thick-skinned structures in the interior of the Idaho-Montana fold-thrust belt (Figure 1) suggests a regional basal detachment within the deeper crust (Figures 11c), most likely rooted near the brittle-plastic transition. We schematically show this detachment between the middle and upper crust (Figures 11c), which is consistent with depth-to-detachment estimates for the Blacktail-Snowcrest uplift in southwestern Montana (McBride et al., 1992) as well as better-constrained structures in Wyoming (e.g., Groshong & Porter, 2019; Smithson et al., 1979; Yeck et al., 2014). Note that we expect the former (T_1) and later (T_2) basal detachment horizons to be closer together in the hinterland and farther from one another in the foreland (red boxes in Figures 11c). This is expected for two reasons. First, in retroarc fold-thrust belts, the hinterland usually contains a relatively thick pre-thrusting stratigraphic section with the mechanical basement-cover contact occurring near or below the brittle-plastic transition. Second, increased temperatures due to crustal thickening in the internal part of the orogenic wedge generally increase hinterland geothermal gradients, resulting in a decrease in the depth of the brittle-plastic transition with progressive orogenesis. Both of these reasons mean that the foreland has more mechanical basement and fewer weak stratigraphic units, making the progressive down-stepping and change in structural style more pronounced in the foreland as compared to the hinterland (Figures 11c). This integrated double-decker system is supported by available kinematic data for thick-skinned thrusts in southwestern Montana that constrain regional E-W shortening and demonstrate strain compatibility with thin-skinned thrusts in the region (O'Neill et al., 1990; Schmidt & Garihan, 1983; Schmidt, O'Neill, & Brandon, 1988).

While a general transition from thin-skinned to thick-skinned thrusting is well documented, observations of mutually cross-cutting thin-skinned and thick-skinned structures in the Idaho-Montana fold-thrust belt suggest that in detail this transition in structural style was not sharp in time or space. For instance, the basal detachment of the Tendoy thrust truncated older folds that were inferred to be related to the Blacktail-Snowcrest arch, a major thick-skinned thrust of the region (McDowell, 1997). Studies within the foreland basin of southwestern Montana suggest that activity along similar low-magnitude, thick-skinned thrusts preceded the peak of thin-skinned thrusting (Decelles, 1986; Garber et al., 2020; Perry et al., 1988). These examples of early, minor thick-skinned thrusts may signify that stress is more efficiently transferred along viscous detachment horizons within the middle crust as compared to frictional detachment horizons of the upper crust (Borderie et al., 2018; Ruh et al., 2012; Tavani et al., 2021). Strain may also be transferred gradually or shared between the upper thin-skinned and lower thick-skinned basal detachments as has been documented in the Zagros fold-thrust belt (e.g., Mouthereau, Lacombe, Vergés, 2012). With more shortening, strain is completely transferred from the upper to the lower basal detachment as out-of-sequence thick-skinned thrusts completely crosscut older and higher thin-skinned thrusts (Figures 11c). A similar progressive shift from early thin-skinned to late thick-skinned deformation has been documented in the fold-thrust belts of the Zagros, Appennines, Oman, and Taiwan, where the inherited rift architecture limits the availability of brittle and plastic detachment horizons (Tavani et al., 2021). Like the Idaho-Montana fold-thrust belt, these examples also suggest that activation of a viscous detachment within the middle crust resulted in rapid propagation of early thick-skinned deformation and that ultimately the former upper thin-skinned belt was overprinted by the lower thick-skinned system as it became dominant (Tavani et al., 2021).

The double-decker model applies to fold-thrust belts in which a critically tapered wedge cannot be contained within only sedimentary cover rocks. Thick-skinned thrusts beneath overlying older thin-skinned thrusts provide a way to thicken the wedge with minimal horizontal shortening. The initial geometry of

the basement-cover contact, which in the current study is a result of heterogeneities during prior rifting (Brennan et al., 2020), determines where structural style will transition from thin-skinned to thick-skinned. Thick-skinned thrusting initiates as a more effective way to build structural relief, without large-magnitude horizontal shortening. With enough horizontal shortening, a self-organized transition from thin-skinned to thick-skinned thrusting occurs near thin, shallow, and laterally discontinuous stratigraphy. This double-decker model suggests that the preexisting distribution of weak stratigraphic layers may determine structural style. Further, this depth-dependent model not only more accurately represents the three-dimensional geometry of structural domains, it may also be a more predictive way to integrate a bewildering range of structural styles into a coherent set of deformation events independent of assumptions about plate boundary geodynamics.

5.4. Implications of the Double-Decker Model

Several different models may explain the occurrence of both thin-skinned and thick-skinned thrusts within a given area (Figure 1). Each model makes unique predictions about shortening magnitude and strain compatibility, both of which greatly impact our understanding of plate dynamics in orogenic belts. In the North and South American Cordilleras, many workers have described fold-thrust belts with discrete thin-skinned and thick-skinned thrust domains in map and cross-section view (Figure 1c; e.g., Armstrong, 1968; Jordan & Allmendinger, 1986). In the thin-skinned domain, structural relief is achieved by major horizontal shortening (e.g., DeCelles, 2004), whereas in the thick-skinned domain, low magnitudes of horizontal shortening on steep basement ramps more efficiently produce structural relief (e.g., Erslev, 1986). In this view, each thin-skinned or thick-skinned domain has distinctive basal detachment horizons with different strain fields (Figure 1c), which are often interpreted to reflect changes in plate boundary geodynamics (e.g., Erslev, 1993; Hamilton, 1988; Yonkee & Weil, 2015). This model works well for the classic Laramide province in the North American Cordillera and in central Argentina, where there is abundant independent evidence of flat-slab subduction that matches the timing and distribution of thick-skinned deformation (e.g., Anderson et al., 2007; Bird, 1988; Coney & Reynolds, 1977; DeCelles, 2004; Dickinson & Snyder, 1978; Jordan & Allmendinger, 1986; Jordan et al., 1983; Kay et al., 1987; Liu et al., 2010; Saleeby, 2003; Yonkee & Weil, 2015). But this model, which suggests a direct link between a shallowly subducting oceanic plate and thick-skinned deformation in the upper plate, is not sufficient in other localities. For example, in the Idaho-Montana fold-thrust belt, thick-skinned thrusts are 10 s of m.y. older than predicted (e.g., Carrapa et al., 2019; Garber et al., 2020; Perry et al., 1988), and magmatism apparently remained active in the hinterland (e.g., Gaschnig, Vervoort, Lewis, & McClelland, 2010; Gaschnig, Vervoort, Lewis, & Tikoff, 2011). Similarly, in northwestern Argentina, active basement-involved, thick-skinned deformation occurs nearly 500 km north (e.g., Allmendinger et al., 1983; Kley et al., 1999; Pearson et al., 2013) of the modern region of shallow subduction (Anderson et al., 2007).

If thick-skinned and thin-skinned thrusts are kinematically linked (Figures 1a and 1b), then spatial heterogeneities in the mechanical properties of the deforming lithosphere offer a more appealing control on structural style than a change in plate boundary geodynamics. At the scale of a single major thrust, one example of how this may occur is where slip along thick-skinned thrusts is transferred to bedding-parallel thrusts (Figure 1a; e.g., uncoupled basement-cover bonding model of Giambiagi et al. [2009]). This model is similar to the synclinal crowding case of trishear fault-propagation folding (Erslev, 1991; Von Hagke & Malz, 2018), a basement-involved wedge structure (Mount et al., 2011), or fault-bend fold (Suppe, 1983). In these examples, a continuum of thin-skinned and thick-skinned structures results from slip along a single basal detachment horizon that passes through a heterogeneous mechanical stratigraphy and strain is transferred into thin-skinned thrusts with comparable slip but less structural relief.

At broader, regional, and orogenic scales, our double-decker model predicts a continuum of structural styles that do not clearly delineate thin-skinned and thick-skinned map domains, suggesting that plate boundary geodynamics cannot be inferred from structural style alone. Structural style is instead time-dependent and depth-dependent, and ultimately determined by the pre-thrusting mechanical stratigraphy and a basal detachment horizon that steps to deeper structural levels with progressive deformation. As a result, younger and more deeply detached structures of one style may crosscut older and more shallowly detached structures of another style while forming in response to the same evolving stress field. Shortening directions

may be refracted around preexisting structures, but highlight an overall regional trend (e.g., Erslev & Koenig, 2009; Schmidt & Garihan, 1983; Weil & Yonkee, 2012; Weil, Yonkee, & Kendall, 2014). In this way, local mechanical stratigraphy determines structural style, but regional trends in the pre-thrusting stratigraphy determine how the host of resulting structural styles may be linked across the orogenic wedge at a given time. These factors, in addition to the natural tendency of basal detachment horizons—particularly near the front of the orogenic wedge—to get deeper with time, may result in changes in the orogenic wedge's ability to shorten. A likely scenario is that early thin-skinned deformation may easily accommodate large magnitudes of horizontal shortening, but give way to later thick-skinned deformation that more effectively builds structural relief as higher-angle thrust ramps cut mechanical basement and uplift portions of the former overlying thin-skinned belt. The double-decker model also predicts that the pre-thrusting mechanical stratigraphy has a stronger control on the geometry, kinematics, and magnitude of shortening in continental fold-thrust belts than previously appreciated: the mechanical properties of the upper plate may not only explain the continuum of structural styles observed in Cordilleran systems, but they may also effectively modulate an orogenic wedge's ability to shorten and thicken in a self-organized way.

6. Conclusions

Mapping and structural analysis in the Beaverhead Mountains of east-central Idaho defines an early, thin-skinned thrust system in sedimentary cover rocks and a late, out-of-sequence thick-skinned thrust system in the underlying mechanical basement of the Lemhi arch. Early detachment folding accommodated NE-SW shortening of the ~3.5-km-thick sedimentary cover rocks. Thin-skinned top-to-the-east thrusting accommodated by the Thompson Gulch and Railroad Canyon thrusts cut across the sedimentary cover rocks, producing carbonate mylonite. Basement and deformed cover rocks were then tilted 5°–15° toward the southeast as a basal detachment in the mechanical basement was activated. Finally, reactivation of an inherited, pre-thrusting normal fault resulted in thick-skinned thrusting of the Baby Joe Gulch, Radio Tower, and Italian Gulch thrusts, which shortened the underlying mechanical basement and cover by at least ~2 km, crosscutting earlier thin-skinned thrusts in the tilted section. Progressive down-stepping of the basal detachment crossed the basement/cover contact near the thin, shallow, and discontinuous stratigraphy overlying the basement high, thereby shifting the structural style from thin-skinned to thick-skinned. This stratigraphically controlled transition to thick-skinned thrusting occurred at depths of 6–9 km, greater than 50 km inboard from thick-skinned thrusts of the southwestern Montana foreland. We propose a double-decker model that predicts a shift from an upper thin-skinned to a lower thick-skinned domain where and when the height of the critically tapered wedge exceeds the thickness of sedimentary cover rocks. This predictive depth-dependent model may aid in integrating thin-skinned and thick-skinned domains of continental fold-thrust belts into a single deformation history where the thickness and lateral continuity of weak sedimentary rocks determine the structural style.

Data Availability Statement

Data supporting the conclusions are available in the accompanying text and figures and can be accessed in the Dryad data repository (https://doi.org/10.5061/dryad.3bk3j9kjx). Additional data were not used, nor created for this research.

Acknowledgments
This study represents a portion of S. D. Parker's PhD dissertation. The authors thank Leif Tapanila for assistance with fossil identification and Paul Link for feedback on early map and manuscript drafts. D. M. Pearson thanks Tom Becker for discussions about structural style. Funding for this research was provided by NSF-Tectonics EAR-1728563 to D. M. Pearson. The authors appreciate critical and constructive reviews by Dr. John Singleton, Dr. Arlo Weil, and an anonymous reviewer, as well as suggestions from the Associate Editor Dr. Elisa Fitz-Díaz and Editor Dr. Margaret Rusmore.

References

Allen, M. B., Saville, C., Blanc, E. J.-P., Talebian, M., & Nissen, E. (2013). Orogenic plateau growth: Expansion of the Turkish-Iranian Plateau across the Zagros fold-and-thrust belt. *Tectonics*, *32*, 171–190. https://doi.org/10.1002/tect.20025

Allmendinger, R. W., Cardozo, N. C., & Fisher, D. (2013). *Structural geology algorithms: Vectors & tensors*. Cambridge University Press.

Allmendinger, R. W., & Gubbels, T. (1996). Pure and simple shear plateau uplift, Altiplano-Puna, Argentina and Bolivia. *Tectonophysics*, *259*(1–3), 1–13. https://doi.org/10.1016/0040-1951(96)00024-8

Allmendinger, R. W., Hauge, T. A., Hauser, E. C., Potter, C. J., Klemperer, S. L., Nelson, K. D., et al. (1987). Overview of the COCORP 40°N Transect, western United States: The fabric of an orogenic belt. *Geological Society of America Bulletin*, *98*(3), 308–319. https://doi.org/10.1130/0016-7606(1987)98<308:OOTCNT>2.0.CO;2

Allmendinger, R. W., Ramos, V. A., Jordan, T. E., Palma, M., & Isacks, B. L. (1983). Paleogeography and Andean structural geometry, northwest Argentina. *Tectonics*, *2*(1), 1–16. https://doi.org/10.1029/TC002i001p00001

Anastasio, D. J., Fisher, D. M., Messina, T. A., & Holl, J. E. (1997). Kinematics of décollement folding in the Lost River Range, Idaho. *Journal of Structural Geology*, *19*(3–4), 355–368. https://doi.org/10.1016/S0191-8141(97)83028-3

Anderson, M., Alvarado, P., Zandt, G., & Beck, S. (2007). Geometry and brittle deformation of the subducting Nazca Plate, Central Chile and Argentina. *Geophysical Journal International*, *171*(1), 419–434. https://doi.org/10.1111/j.1365-246X.2007.03483.x

Armstrong, R. L. (1968). Sevier orogenic belt in Nevada and Utah. *Geological Society of America Bulletin*, *79*(4), 429–458. https://doi.org/10.1130/0016-7606(1968)79[429:SOBINA]2.0.CO;2

Armstrong, R. L., & Dick, H. J. B. (1974). A model for the development of thin overthrust sheets of crystalline rock. *Geology*, *2*(1), 35–40. https://doi.org/10.1130/0091-7613(1974)2%3C35:AMFTDO%3E2.0.CO;2

Baby, P., Moretti, I., Guillier, B., Limachi, R., Mendez, E., Oller, J., & Specht, M. (1995). Petroleum system of the northern and central Bolivian sub-Andean zone. In A. J. Tankard, R. Suarez Soruco, & H. J. Welsink (Eds.), *Petroleum basins of south America* (Vol. 62). American Association of Petroleum Geologists Memoir.

Bally, A. W., Gordy, P. L., & Stewart, G. A. (1966). Structure, seismic data, and orogenic evolution of southern Canadian Rocky Mountains. *Bulletin of Canadian Petroleum Geology*, *14*(3), 337–381. https://doi.org/10.35767/gscpgbull.14.3.337

Barnhart, W. D., Brengman, C. M. J., Li, S., & Peterson, K. E. (2018). Ramp-flat basement structures of the Zagros Mountains inferred from co-seismic slip and afterslip of the 2017 Mw7.3 Darbandikhan, Iran/Iraq earthquake. *Earth and Planetary Science Letters*, *496*, 96–107. https://doi.org/10.1016/j.epsl.2018.05.036

Bauville, A., & Schmalholz, S. M. (2015). Transition from thin- to thick-skinned tectonics and consequences for nappe formation: Numerical simulations and applications to the Helvetic nappe system, Switzerland. *Tectonophysics*, *665*, 101–117. https://doi.org/10.1016/j.tecto.2015.09.030

Bell, T. H., & Etheridge, M. A. (1973). Microstructure of mylonites and their descriptive terminology. *Lithos*, *6*(4), 337–348. https://doi.org/10.1016/0024-4937(73)90052-2

Betka, P., Klepeis, K., & Mosher, S. (2015). Along-strike variation in crustal shortening and kinematic evolution of the base of a retroarc fold-and-thrust belt: Magallanes, Chile 53°S-54°S. *Geological Society of America Bulletin*, *127*(7–8), 1108–1134. https://doi.org/10.1130/B31130.1

Beutner, E. C. (1968). *Structure and tectonics of the southern Lemhi Range, Idaho* (Doctoral dissertation). Pennsylvania State University.

Bird, P. (1988). Formation of the Rocky Mountains, western United States: A continuum computer model. *Science*, *239*(4847), 1501–1507. https://doi.org/10.1126/science.239.4847.1501

Blackstone, D. L., Jr. (1940). Structure of the Pryor Mountains Montana. *The Journal of Geology*, *48*(6), 590–618. https://doi.org/10.1086/624917

Borderie, S., Graveleau, F., Witt, C., & Vendeville, B. C. (2018). Impact of an interbedded viscous décollement on the structural and kinematic coupling in fold-and-thrust belts: Insights from analogue modeling. *Tectonophysics*, *722*, 118–137. https://doi.org/10.1016/j.tecto.2017.10.019

Boyer, S. E. (1995). Sedimentary basin taper as a factor controlling the geometry and advance of thrust belts. *American Journal of Science*, *295*(10), 1220–1254. https://doi.org/10.2475/ajs.295.10.1220

Boyer, S. E., & Elliott, D. (1982). Thrust systems. *The American Association of Petroleum Geologists Bulletin*, *66*(9), 1196–1230. https://doi.org/10.1306/03B5A77D-16D1-11D7-8645000102C1865D

Brennan, D. T., Pearson, D. M., Link, P. K., & Chamberlain, K. R. (2020). Neoproterozoic Windermere Supergroup near Bayhorse, Idaho: Late-stage Rodinian rifting was deflected west around the Belt basin. *Tectonics*, *39*(8), 1–27. https://doi.org/10.1029/2020TC006145

Brumbaugh, D. S., & Hendrix, T. E. (1981). The McCarthy Mountain structural salient southwestern Montana. In *Montana Geological Society field conference & symposium guidebook to southwest Montana* (pp. 201–210). Montana Geological Society.

Buiter, S. J. H. (2012). A review of brittle compressional wedge models. *Tectonophysics*, *530–531*, 1–17. https://doi.org/10.1016/j.tecto.2011.12.018

Burchfiel, B. C., & Davis, G. A. (1972). Structural framework and evolution of the southern part of the Cordilleran orogen, western United States. *American Journal of Science*, *272*(2), 97–118. https://doi.org/10.2475/ajs.272.2.97

Burchfiel, B. C., & Davis, G. A. (1975). Nature and controls of Cordilleran orogenesis, western United States: Extensions of an earlier synthesis. *American Journal of Science*, *275*(A), 363–396. https://doi.org/10.2475/ajs.275.8.987

Burkhard, M. (1990). Ductile deformation mechanisms in micritic limestones naturally deformed at low temperatures (150-350°C). *Geological Society of London*, *54*(1), 241–257. https://doi.org/10.1144/GSL.SP.1990.054.01.23

Burkhard, M. (1993). Calcite twins, their geometry, appearance and significance as stress-strain markers and indicators of tectonic regime: A review. *Journal of Structural Geology*, *15*(3–5), 351–368. https://doi.org/10.1016/0191-8141(93)90132-T

Butler, R. W. H., Bond, C. E., Cooper, M. A., & Watkins, H. (2018). Interpreting structural geometry in fold-thrust belts: Why style matters. *Journal of Structural Geology*, *114*, 251–273. https://doi.org/10.1016/j.jsg.2018.06.019

Carney, S. M., & Janecke, S. U. (2005). Excision and the original low dip of the Miocene-Pliocene Bannock detachment system, SE Idaho: Northern cousin of the Sevier Desert detachment? *Geological Society of America Bulletin*, *117*(3–4), 334–353. https://doi.org/10.1130/B25428.1

Carrapa, B., DeCelles, P. G., & Romero, M. (2019). Early inception of the Laramide orogeny in southwestern Montana and northern Wyoming: Implications for models of flat-slab subduction. *Journal of Geophysical Research: Solid Earth*, *124*(2), 2102–2123. https://doi.org/10.1029/2018JB016888

Chapman, J. B., & DeCelles, P. G. (2015). Foreland basin stratigraphic control on thrust belt evolution. *Geology*, *43*(7), 579–582. https://doi.org/10.1130/G36597.1

Coney, P. J., & Reynolds, S. J. (1977). Cordilleran benioff zones. *Nature*, *270*(5636), 403–406. https://doi.org/10.1038/270403a0

Coogan, J. C. (1992). Chapter 2: Structural evolution of piggyback basins in the Wyoming-Idaho-Utah thrust belt. In P. K. Link, M. A. Kuntz, & L. B. Piatt (Eds.), *Regional geology of eastern Idaho and western Wyoming* (Vol. 179, pp. 55–82). Geological Society of America Memoir. https://doi.org/10.1130/MEM179-p55

Cook, F. A., & Varsek, J. L. (1994). Orogen-scale decollements. *Reviews of Geophysics*, *32*(1), 37–60. https://doi.org/10.1029/93rg02515

Dahlstrom, C. D. (1970). Structural geology in the eastern margin of the Canadian Rocky Mountains. *Bulletin of Canadian Petroleum Geology*, *18*(3), 332–406.

Davis, D. M., & Engelder, T. (1985). The role of salt in fold-and-thrust belts. *Tectonophysics*, *119*, 67–88. https://doi.org/10.1016/0040-1951(85)90033-2

Davis, D., Suppe, J., & Dahlen, F. A. (1983). Mechanics of fold-and-thrust belts and accretionary wedges. *Journal of Geophysical Research*, *88*(B2), 1153–1172. https://doi.org/10.1029/JB088iB02p01153

De Bresser, J. H. P., Evans, B., & Renner, J. (2002). On estimating the strength of calcite rocks under natural conditions. *Geological Society of London*, *200*(1), 309–329. https://doi.org/10.1144/GSL.SP.2001.200.01.18

Decelles, P. G. (1986). Sedimentation in a tectonically partitioned, nonmarine foreland basin: The Lower Cretaceous Kootenai Formation, southwestern Montana. *Geological Society of America Bulletin*, *97*(8), 911–931. https://doi.org/10.1130/0016-7606(1986)97<911:SIATPN>2.0.CO;2

DeCelles, P. G. (1994). Late Cretaceous-Paleocene synorogenic sedimentation and kinematic history of the Sevier thrust belt, northeast Utah and southwest Wyoming. *Geological Society of America Bulletin*, *106*(1), 32–56. https://doi.org/10.1130/0016-7606(1994)106<0032:LCPSSA>2.3.CO;2

DeCelles, P. G. (2004). Late Jurassic to Eocene evolution of the Cordilleran thrust belt and foreland basin system, western U.S.A. *American Journal of Science*, *304*(2), 105–168. https://doi.org/10.2475/ajs.304.2.105

DeCelles, P. G., & Coogan, J. C. (2006). Regional structure and kinematic history of the Sevier fold-and-thrust belt, central Utah. *Geological Society of America Bulletin*, *118*(7–8), 841–864. https://doi.org/10.1130/B25759.1

DeCelles, P. G., Lawton, T. F., & Mitra, G. (1995). Thrust timing, growth of structural culminations, and synorogenic sedimentation in the type Sevier orogenic belt, western United States. *Geology*, *23*(8), 699–702. https://doi.org/10.1130/0091-7613(1995)023<0699:TTGOSC>2.3.CO;2

DeCelles, P. G., & Mitra, G. (1995). History of the Sevier orogenic wedge in terms of critical taper models, northeast Utah and southwest Wyoming. *Geological Society of America Bulletin*, *107*(4), 454–462. https://doi.org/10.1130/0016-7606(1995)107<0454:HOTSOW>2.3.CO;2

DeCelles, P. G., Robinson, D. M., Quade, J., Ojha, T. P., Garzione, C. N., Copeland, P., & Upreti, B. N. (2001). Stratigraphy, structure, and tectonic evolution of the Himalayan fold-thrust belt in western Nepal. *Tectonics*, *20*(4), 487–509. https://doi.org/10.1029/2000TC001226

Dembicki, H. (2016). *Practical petroleum geochemistry for exploration and production*. Elsevier.

Dickinson, W. R., & Snyder, W. S. (1978). Plate tectonics of the Laramide orogeny. In V. Matthews (Ed.), *Laramide folding associated with basement block faulting in the western United States* (Vol. 151, pp. 355–366). Geological Society of America Memoir. https://doi.org/10.1130/MEM151-p355

Dover, J. H. (1981). Geology of the Boulder-Pioneer wilderness study area. Blaine and Custer Counties, Idaho. *US Geological Survey Bulletin*, *1497*, 15–75.

Dunn, J. F., Hartshorn, K. G., & Hartshorn, P. W. (1995). Structural styles and hydrocarbon potential of the sub-Andean thrust belt of southern Bolivia. In A. J. Tankard, R. Suarez Soruco, & H. J. Welsink (Eds.), *Petroleum basins of south America* (Vol. 62). American Association of Petroleum Geologists Memoir.

Eardley, A. J. (1963). Relation of uplifts to thrusts in Rocky Mountains. In O. E. Childs, & B. W. Beebe (Eds.), *Backbone of the Americas: Tectonic history from pole to pole* (Vol. 2, pp. 209–219). Rocky Mountain Association of Geologists.

Echavarria, L., Hernández, R., Allmendinger, R., & Reynolds, J. (2003). Subandean thrust and fold belt of northwestern Argentina: Geometry and timing of the Andean evolution. *AAPG Bulletin*, *87*(6), 965–985. https://doi.org/10.1306/01200300196

Erslev, E. A. (1986). Basement balancing of Rocky Mountain foreland uplifts. *Geology*, *14*(3), 259–262. https://doi.org/10.1130/0091-7613(1986)14<259:BBORMF>2.0.CO;2

Erslev, E. A. (1991). Trishear fault-propagation folding. *Geology*, *19*(6), 617–620. https://doi.org/10.1130/0091-7613(1991)019<0617:TFPF>2.3.CO;2

Erslev, E. A. (1993). Thrusts, back-thrusts, and detachment of Rocky Mountain foreland arches. In C. J. Schmidt, R. B. Chase, & E. A. Erslev (Eds.), *Laramide basement deformation in the Rocky Mountain foreland of the western United States* (Vol. 280, pp. 339–358). Geological Society of America Special Paper. https://doi.org/10.1130/SPE280-p339

Erslev, E. A., & Koenig, N. V. (2009). Three-dimensional kinematics of Laramide, basement-involved Rocky Mountain deformation, USA: Insights from minor faults and GIS-enhanced structure maps. In S. M. Kay, V. A. Ramos, & W. R. Dickinson (Eds.), *Backbone of the Americas: Shallow subduction, plateau uplift, and ridge and terrane collision* (Vol. 204, pp. 125–150). Geological Society of America Memoirs. https://doi.org/10.1130/2009.1204(06)

Evans, K. V., & Green, G. N. (2003). *Geologic map of the Salmon National Forest and vicinity, east-central Idaho* (Geological Investigation Series Map I-2765, scale 1:100,000). U.S. Geological Survey.

Evans, K. V., & Zartman, R. E. (1988). Early Paleozoic alkalic plutonism in east-central Idaho. *Geological Society of America Bulletin*, *100*(12), 1981–1987. https://doi.org/10.1130/0016-7606(1988)100<1981:EPAPIE>2.3.CO;2

Fermor, P. R., & Moffat, I. W. (1992). The Cordilleran collage and the foreland fold and thrust belt. In R. W. MacQueen, & D. A. Leckie (Eds.), *Foreland basins and fold belts* (Vol. 55, pp. 81–105). American Association of Petroleum Geologists.

Ferrill, D. A., Morris, A. P., Evans, M. A., Burkhard, M., Groshong, R. H., Jr., & Onasch, C. M. (2004). Calcite twin morphology: A low-temperature deformation geothermometer. *Journal of Structural Geology*, *26*(8), 1521–1529. https://doi.org/10.1016/j.jsg.2003.11.028

Fitz-Díaz, E., Lawton, T. F., Juárez-Arriaga, E., & Chávez-Cabello, G. (2018). The Cretaceous-Paleogene Mexican orogen: Structure, basin development, magmatism and tectonics. *Earth-Science Reviews*, *183*, 56–84. https://doi.org/10.1016/j.earscirev.2017.03.002

Fossen, H. (2016). Structural geology (Vol. 2). Cambridge University Press.

Fuentes, F., Horton, B. K., Starck, D., & Boll, A. (2016). Structure and tectonic evolution of hybrid thick- and thin-skinned systems in the Malargüe fold-thrust belt, Neuquén basin, Argentina. *Geological Magazine*, *153*(5–6), 1066–1084. https://doi.org/10.1017/S0016756816000583

Garber, K. L., Finzel, E. S., & Pearson, D. M. (2020). Provenance of synorogenic foreland basin strata in southwestern Montana requires revision of existing models for laramide tectonism: North American Cordillera. *Tectonics*, *39*(2), 1–26. https://doi.org/10.1029/2019TC005944

Gaschnig, R. M., Vervoort, J. D., Lewis, R. S., & McClelland, W. C. (2010). Migrating magmatism in the northern US Cordillera: In situ U-Pb geochronology of the Idaho batholith. *Contributions to Mineralogy and Petrology*, *159*(6), 863–883. https://doi.org/10.1007/s00410-009-0459-5

Gaschnig, R. M., Vervoort, J. D., Lewis, R. S., & Tikoff, B. (2011). Isotopic evolution of the Idaho batholith and Challis intrusive province, northern US Cordillera. *Journal of Petrology*, *52*(12), 2397–2429. https://doi.org/10.1093/petrology/egr050

Giambiagi, L., Bechis, F., García, V., & Clark, A. H. (2008). Temporal and spatial relationships of thick- and thin-skinned deformation: A case study from the Malargüe fold-and-thrust belt, southern Central Andes. *Tectonophysics*, *459*(1–4), 123–139. https://doi.org/10.1016/j.tecto.2007.11.069

Giambiagi, L., Ghiglione, M., Cristallini, E., & Bottesi, G. (2009). Kinematic models of basement/cover interaction: Insights from the Malargüe fold and thrust belt, Mendoza, Argentina. *Journal of Structural Geology*, *31*(12), 1443–1457. https://doi.org/10.1016/j.jsg.2009.10.006

Giambiagi, L., Mescua, J., Bechis, F., Tassara, A., & Hoke, G. (2012). Thrust belts of the southern Central Andes: Along-strike variations in shortening, topography, crustal geometry, and denudation. *Geological Society of America Bulletin*, *124*(7–8), 1339–1351. https://doi.org/10.1130/B30609.1

Goscombe, B. D., Passchier, C. W., & Hand, M. (2004). Boudinage classification: End-member boudin types and modified boudin structures. *Journal of Structural Geology*, *26*(4), 739–763. https://doi.org/10.1016/j.jsg.2003.08.015

Grader, G. W., & Dehler, C. M. (1999). Devonian stratigraphy in east-central Idaho: New perspectives from the Lemhi Range and Bayhorse area. In S. S. Hughes & G. D. Thackray (Eds.), *Guidebook to the geology of eastern Idaho* (pp. 31–56). Idaho Museum of Natural History & Idaho State University Press.

Grader, G. W., Isaacson, P. E., Doughty, P. T., Pope, M. C., & Desantis, M. K. (2017). Idaho Lost River shelf to Montana craton: North American Late Devonian stratigraphy, surfaces, and intrashelf basin. In T. E. Playton, C. Kerans, & A. W. Weissenberger (Eds.), *New advances in Devonian Carbonates: Outcrop analogs, reservoirs, and chronostratigraphy* (Vol. 107, pp. 347–379). Society for Sedimentary Geology Special Publication. https://doi.org/10.2110/sepmsp.107.12

Graveleau, F., Malavieille, J., & Dominguez, S. (2012). Experimental modelling of orogenic wedges: A review. *Tectonophysics*, *538–540*, 1–66. https://doi.org/10.1016/j.tecto.2012.01.027

Gray, G., Zhang, Z., & Barrios, A. (2019). Basement-involved, shallow detachment faulting in the Bighorn Basin, Wyoming and Montana. *Journal of Structural Geology*, *120*, 80–86. https://doi.org/10.1016/j.jsg.2018.10.015

Groshong, R. H., & Porter, R. (2019). Predictive models for the deep geometry of a thick-skinned thrust matched to crustal structure: Wind River Range, western USA. *Lithosphere*, *11*(4), 448–464. https://doi.org/10.1130/L1031.1

Hait, Jr. M. H. (1965). *Structure of the Gilmore area, Lemhi range, Idaho* (Doctoral dissertation). Pennsylvania State University.

Haley, J. C., Bonilla, M. G., Meyer, R. F., Yeend, W. E., Lienkaemper, J. J., & Perry, W. J. (1991). The Red Butte Conglomerate: A thrust-belt-derived conglomerate of the Beaverhead Group, southwestern Montana. *US Geological Survey Bulletin*, *1945*, 1–19.

Hamilton, W. B. (1988). Laramide crustal shortening. *Geological Society of America Memoir*, *171*, 27–40. https://doi.org/10.1130/MEM171-p27

Hansen, C. M., & Pearson, D. M. (2016). *Geologic map of the Poison Creek thrust fault and vicinity near Poison Peak and Twin Peaks, Lemhi County, Idaho* (Technical Report T-16-1, scale 1:24,000). Idaho Geological Survey.

Huh, O. K. (1967). The Mississippian system across the Wasatch line east central Idaho, extreme southwestern Montana. In *Montana geological society 18th annual field conference 1967* (pp. 31–62). Montana Geological Society.

Hung, J.-H., Wiltschko, D. V., Lin, H.-C., Hickman, J. B., Fang, P., & Bock, Y. (1999). Structure and motion of the southwestern Taiwan fold and thrust belt. *Terrestrial, Atmospheric and Oceanic Sciences*, *10*, 543–568. https://doi.org/10.3319/TAO.1999.10.3.543(T)

James, W. C., & Oaks, R. Q. (1977). Petrology of the Kinnikinic Quartzite (Middle Ordovician), east-central Idaho. *Journal of Sedimentary Research*, *47*(4), 1491–1511. https://doi.org/10.1306/212F73A1-2B24-11D7-8648000102C1865D

Janecke, S. U., VanDenburg, C. J., Blankenau, J. J., & M'Gonigle, J. W. (2000). Long-distance longitudinal transport of gravel across the Cordilleran thrust belt of Montana and Idaho. *Geology*, *28*(5), 439–442. https://doi.org/10.1130/0091-7613(2000)28<439:LLTOGA>2.0.CO;2

Jordan, T. E., & Allmendinger, R. W. (1986). The Sierras Pampeanas of Argentina; A modern analogue of Rocky Mountain foreland deformation. *American Journal of Science*, *286*(10), 737–764. https://doi.org/10.2475/ajs.286.10.737

Jordan, T. E., Isacks, B. L., Allmendinger, R. W., Brewer, J. A., Ramos, V. A., & Ando, C. J. (1983). Andean tectonics related to geometry of subducted Nazca plate. *Geological Society of America Bulletin*, *94*(3), 341–361. https://doi.org/10.1130/0016-7606(1983)94<341:ATRTGO>2.0.CO;2

Kay, M. (1951). North American geosynclines (Vol. 48). Geological Society of America Memoir. https://doi.org/10.1130/MEM48

Kay, S. M., Maksaev, V., Moscoso, R., Mpodozis, C., & Nasi, C. (1987). Probing the evolving Andean Lithosphere: Mid-Late Tertiary magmatism in Chile (29°-30°30′S) over the modern zone of subhorizontal subduction. *Journal of Geophysical Research*, *92*(B7), 6173–6189. https://doi.org/10.1029/JB092iB07p06173

Kley, J. (1996). Transition from basement-involved to thin-skinned thrusting in the Cordillera Oriental of southern Bolivia. *Tectonics*, *15*(4), 763–775. https://doi.org/10.1029/95TC03868

Kley, J., & Monaldi, C. R. (2002). Tectonic inversion in the Santa Barbara System of the central Andean foreland thrust belt, northwestern Argentina. *Tectonics*, *21*(6), 11–1. https://doi.org/10.1029/2002TC902003

Kley, J., Monaldi, C. R., & Salfity, J. A. (1999). Along-strike segmentation of the Andean foreland: Causes and consequences. *Tectonophysics*, *301*(1–2), 75–94. https://doi.org/10.1016/S0040-1951(98)90223-2

Krumbein, W. C. (1939). Preferred orientation of pebbles in sedimentary deposits. *The Journal of Geology*, *47*(7), 673–706. https://doi.org/10.1086/624827

Kulik, D. M., & Schmidt, C. J. (1988). Region of overlap and styles of interaction of Cordilleran thrust belt and Rocky Mountain foreland. In J. Schmidt & W. J. Perry (Eds.), *Interaction of the Rocky Mountain foreland and the Cordilleran thrust belt* (Vol. 171, pp. 75–98). Geological Society of America Memoir. https://doi.org/10.1130/MEM171-p75

Kuntz, M. A., Skipp, B., Lanphere, M. A., Scott, W. E., Pierce, K. L., Dalrymple, G. B., et al. (1994). *Geologic map of the Idaho National Engineering Laboratory and adjoining areas, eastern Idaho* (Miscellaneous Investigations Series Map I-2330, scale 1:100,000). U.S. Geological Survey.

Lacombe, O., & Bellahsen, N. (2016). Thick-skinned tectonics and basement-involved fold-thrust belts: Insights from selected Cenozoic orogens. *Geological Magazine*, *153*(5–6), 763–810. https://doi.org/10.1017/S0016756816000078

Lacombe, O., & Mouthereau, F. (2002). Basement-involved shortening and deep detachment tectonics in forelands of orogens: insights from recent collision belts (Taiwan, western Alps, Pyrenees). *Tectonics*, *21*, 12–21. https://doi.org/10.1029/2001TC901018

Le Garzic, E., Vergés, J., Sapin, F., Saura, E., Meresse, F., & Ringenbach, J. C. (2019). Evolution of the NW Zagros Fold-and-Thrust Belt in Kurdistan Region of Iraq from balanced and restored crustal-scale sections and forward modeling. *Journal of Structural Geology*, *124*, 51–69. https://doi.org/10.1016/j.jsg.2019.04.006

Link, P. K., Todt, M. K., Pearson, D. M., & Thomas, R. C. (2017). 500-490 Ma detrital zircons in Upper Cambrian Worm Creek and correlative sandstones, Idaho, Montana, and Wyoming: Magmatism and tectonism within the passive margin. *Lithosphere*, *9*(6), 910–926. https://doi.org/10.1130/L671.1

Liu, L., Gurnis, M., Seton, M., Saleeby, J., Müller, R. D., & Jackson, J. M. (2010). The role of oceanic plateau subduction in the Laramide orogeny. *Nature Geoscience*, *3*(5), 353–357. https://doi.org/10.1038/ngeo829

Long, S. (2012). Magnitudes and spatial patterns of erosional exhumation in the Sevier hinterland, eastern Nevada and western Utah, USA: Insights from a Paleogene paleogeologic map. *Geosphere*, *8*(4), 881–901. https://doi.org/10.1130/GES00783.1

Long, S. P., & Kohn, M. J. (2020). Distributed ductile thinning during thrust emplacement: A commonly overlooked exhumation mechanism. *Geology*, *48*(4), 368–373. https://doi.org/10.1130/G47022.1

Lonn, J. D., Burmester, R. F., Lewis, R. S., & McFaddan, M. D. (2016). Giant folds and complex faults in Mesoproterozoic Lemhi strata of the Belt Supergroup, northern Beaverhead Mountains, Montana and Idaho. In J. W. Sears, & J. S. MacLean (Eds.), *Belt basin: Window to Mesoproterozoic Earth* (Vol. 522, pp. 139–162). Geological Society of America Special Paper. https://doi.org/10.1130/2016.2522(06

Lonn, J. D., Elliott, C. G., Stewart, D. E., Mosolf, J. G., Burmester, R. F., Lewis, R. S., & Pearson, D. M. (2019). *Geologic map of the Bannock Pass 7.5′ quadrangle, Beaverhead County, Montana, and Lemhi County, Idaho* (76, scale 1:24,000). Montana Bureau of Mines and Geology.

Lonn, J. D., Skipp, B., Ruppel, E. T., Perry, W. J., Jr., Sears, J. W., Janecke, S. U., et al. (2000). *Geologic map of the Lima 30′ x 60′ quadrangle, southwest Montana* (Open-File Reports 408, scale 1:100,000). Montana Bureau of Mines and Geology.

Lopez, D. A., & Schmidt, C. (1985). Seismic profile across the leading edge of the fold and thrust belt of southwest Montana. In R. R. Gries (Ed.), *Seismic exploration of the Rocky Mountain region* (Vol. 1, pp. 45–50). Rocky Mountain Association of Geologists.

Lovering, T. G. (1962). The origin of jasperoid in limestone. *Economic Geology*, *57*(6), 861–889. https://doi.org/10.2113/gsecongeo.57.6.861

Lucchitta, B. K. (1966). *Structure of the Hawley Creek area, Idaho-Montana* (Doctoral dissertation). Pennsylvania State University. Retrieved from University Microfilms. no. 67-5941.

Lund, K. (2018). *Geologic map of the central Beaverhead Mountains, Lemhi County, Idaho, and Beaverhead County, Montana* (Scientific Investigations Map 3413, scale 1:50,000). U.S. Geological Survey. https://doi.org/10.3133/sim3413

Lund, K., Aleinikoff, J. N., Evans, K. V., DuBray, E. A., Dewitt, E. H., & Unruh, D. M. (2010). SHRIMP U-Pb dating of recurrent Cryogenian and Late Cambrian-Early Ordovician alkalic magmatism in central Idaho: Implications for Rodinian rift tectonics. *Geological Society of America Bulletin*, *122*(3–4), 430–453. https://doi.org/10.1130/B26565.1

Mardia, K. V. (1972). *Statistics of directional data*. Academic Press.

Marshak, S. (2004). Salients, recesses, arcs, oroclines, and syntaxes – A review of ideas concerning the formation of map-view curves in fold-thrust belts. In K. McClay (Ed.), *Thrust tectonics and hydrocarbon systems* (Vol. 82, pp. 131–156). American Association of Petroleum Geologists.

Marshak, S., Karlstrom, K., & Michael Timmons, J. (2000). Inversion of Proterozoic extensional faults: An explanation for the pattern of Laramide and Ancestral Rockies intracratonic deformation, United States. *Geology*, *28*(8), 735–738. https://doi.org/10.1130/0091-7613(2000)28<735:IOPEFA>2.0.CO;2

Martínez, F., Giambiagi, L., Audemard, M. F. A., & Parra, M. (2020). Thrust and fold belts of South America. *Journal of South American Earth Sciences*, *104*, 102822–102823. https://doi.org/10.1016/j.jsames.2020.102822

Mazzotti, S., & Hyndman, R. D. (2002). Yakutat collision and strain transfer across the northern Canadian Cordillera. *Geology*, *30*(6), 495–498. https://doi.org/10.1130/0091-7613(2002)030<0495:YCASTA>2.0.CO;2

McBride, B. C., Schmidt, C. J., Guthrie, G. E., & Sheedlo, M. K. (1992). Multiple reactivation of a collisional boundary: An example from southwestern Montana. In M. J. Bartholomew, D. W. Hyndman, D. Mogk, & R. Mason (Eds.), *Basement tectonics* (Vol. 8, pp. 341–357). Springer. https://doi.org/10.1007/978-94-011-1614-5_23

McDowell, R. J. (1997). Evidence for synchronous thin-skinned and basement deformation in the Cordilleran fold-thrust belt: The Tendoy Mountains, southwestern Montana. *Journal of Structural Geology*, *19*(1), 77–87. https://doi.org/10.1016/S0191-8141(96)00044-2

McGroder, M. F., Lease, R. O., & Pearson, D. M. (2015). Along-strike variation in structural styles and hydrocarbon occurrences, Subandean fold-and-thrust belt and inner foreland, Colombia to Argentina. In P. G. DeCelles, M. N. Ducea, B. Carrapa, & P. A. Kapp (Eds.), *Geodynamics of a cordilleran orogenic system: The central Andes of Argentina and northern Chile* (Vol. 212, pp. 79–113). Geological Society of America Memoir. https://doi.org/10.1130/2015.1212(05

McMechan, M. E., Thompson, R. I., Caldwell, W. G. E., & Kauffman, E. G. (1993). The Canadian Cordilleran fold and thrust belt south of 66 N and its influence on the Western Interior Basin. In W. G. E. Caldwell, & E. G. Kauffman (Eds.), *Evolution of the western interior basin* (Vol. 39, pp. 73–90). Geological Association of Canada.

McQuarrie, N. (2002). The kinematic history of the central Andean fold-thrust belt, Bolivia: Implications for building a high plateau. *Geological Society of America Bulletin*, *114*(8), 950–963. https://doi.org/10.1130/0016-7606(2002)114<0950:TKHOTC>2.0.CO;2

McQuarrie, N. (2004). Crustal scale geometry of the Zagros fold-thrust belt, Iran. *Journal of Structural Geology*, *26*(3), 519–535. https://doi.org/10.1016/j.jsg.2003.08.009

McQueen, H. W. S., & Beaumont, C. (1989). Mechanical models of tilted block basins. In R. A. Price (Ed.), *AGU/IUGG monograph* (Vol. 48, pp. 65–71). https://doi.org/10.1029/GM048p0065

Messina, T. A. (1993). *The geometry and kinematics of intra-thrust sheet decollment folding: Lost River Range, Idaho* (MS thesis). Lehigh University.

M'Gonigle, J. W. (1993). *Geologic map of the Medicine Lodge Peak quadrangle, Beaverhead County, southwest Montana* (Geologic Quadrangle Map GQ-1724, scale 1:24,000). U.S. Geological Survey.

M'Gonigle, J. W. (1994). *Geologic map of the Deadman Pass quadrangle, Beaverhead County, Montana, and Lemhi County, Idaho* (Geologic Quadrangle Map GQ-1753, scale 1:24,000). U.S. Geological Survey.

Mitra, G. (1994). Strain variation in thrust sheets across the Sevier fold-and-thrust belt (Idaho-Utah-Wyoming): Implications for section restoration and wedge taper evolution. *Journal of Structural Geology*, *16*(4), 585–602. https://doi.org/10.1016/0191-8141(94)90099-X

Molinaro, M., Leturmy, P., Guezou, J.-C., Frizon de Lamotte, D., & Eshraghi, S. A. (2005). The structure and kinematics of the southeastern Zagros fold-thrust belt, Iran: From thin-skinned to thick-skinned tectonics. *Tectonics*, *24*(3). https://doi.org/10.1029/2004TC001633

Mount, V. S., Martindale, K. W., Griffith, T. W., & Byrd, J. O. (2011). Basement-involved contractional wedge structural styles: Examples from the Hanna basin, Wyoming. In K. McClay, J. Shaw, & J. Suppe (Eds.), *Thrust fault-related folding* (Vol. 94, pp. 271–281). American Association of Petroleum Geologists. https://doi.org/10.1306/13251341M941003

Mouthereau, F., Lacombe, O., & Meyer, B. (2006). The Zagros Folded Belt (Fars, Iran): Constraints from topography and critical wedge modelling. *Geophysical Journal International*, *165*, 336–356. https://doi.org/10.1111/j.1365-246X.2006.02855.x

Mouthereau, F., Lacombe, O., & Vergés, J. (2012). Building the Zagros collisional orogen: Timing, strain distribution and the dynamics of Arabia/Eurasia plate convergence. *Tectonophysics*, *532–535*, 27–60. https://doi.org/10.1016/j.tecto.2012.01.022

Mouthereau, F., Tensi, J., Bellahsen, N., Lacombe, O., De Boisgrollier, T., & Kargar, S. (2007). Tertiary sequence of deformation in a thin-skinned/thick-skinned collision belt: The Zagros Folded Belt (Fars, Iran). *Tectonics*, *26*(5). https://doi.org/10.1029/2007TC002098

Mouthereau, F., Watts, A. B., & Burov, E. (2013). Structure of orogenic belts controlled by lithosphere age. *Nature Geoscience*, *6*(9), 785–789. https://doi.org/10.1038/ngeo1902

Namson, J. (1981). Structure of the Western Foothills Belt, Miaoli-Hsinchu area, Taiwan: (I) Southern part. *Petroleum Geology of Taiwan*, *18*, 31–51.

Neely, T. G., & Erslev, E. A. (2009). The interplay of fold mechanisms and basement weaknesses at the transition between Laramide basement-involved arches, north-central Wyoming, USA. *Journal of Structural Geology*, *31*(9), 1012–1027. https://doi.org/10.1016/j.jsg.2009.03.008

O'Neill, J. M., Schmidt, C. J., & Genovese, P. W. (1990). Dillon cutoff-Basement-involved tectonic link between the disturbed belt of west-central Montana and the overthrust belt of extreme southwestern Montana. *Geology*, *18*(11), 1107–1110. https://doi.org/10.1130/0091-7613(1990)018<1107:DCBITL>2.3.CO;2

O'Sullivan, P. B., & Wallace, W. K. (2002). Out-of-sequence, basement-involved structures in the Sadlerochit Mountains region of the Arctic National Wildlife Refuge, Alaska: Evidence and implications from fission-track thermochronology. *Geological Society of America Bulletin*, *114*(11), 1356–1378. https://doi.org/10.1130/0016-7606(2002)114<1356:OOSBIS>2.0.CO;2

Parker, S. D., & Pearson, D. M. (2020). *Geologic map of the northern part of the Leadore quadrangle, Lemhi County, Idaho* (Technical Report T-20-03, scale 1:24,000). Idaho Geological Survey.

Pearson, D. M., Kapp, P., DeCelles, P. G., Reiners, P. W., Gehrels, G. E., Ducea, M. N., & Pullen, A. (2013). Influence of pre-Andean crustal structure on Cenozoic thrust belt kinematics and shortening magnitude: Northwestern Argentina. *Geosphere*, *9*(6), 1766–1782. https://doi.org/10.1130/GES00923.1

Pearson, D. M., & Link, P. K. (2017). Field guide to the Lemhi arch and Mesozoic-early Cenozoic faults and folds in east-central Idaho: Beaverhead Mountains. *Northwest Geology*, *46*, 101–112.

Perry, W. J., Jr., Dyman, T. S., & Sando, W. J. (1989). Southwestern Montana recess of Cordilleran thrust belt Montana Geological Society: 1989 field conference guidebook: Montana centennial edition: Geologic resources of Montana (Vol. 1, pp. 261–270). Montana Geological Society.

Perry, W. J., Jr., Haley, J. C., Nichols, D. J., Hammons, P. M., & Ponton, J. D. (1988). Interactions of Rocky Mountain foreland and Cordilleran thrust belt in Lima region, southwest Montana. In J. Schmidt, & W. J. Perry (Eds.), *Interaction of the Rocky Mountain foreland and the Cordilleran thrust belt* (Vol. 171, pp. 267–290). Geological Society of America Memoir. https://doi.org/10.1130/MEM171-p267

Perry, W. J., Jr., & Sando, W. J. (1982). Sequence of deformation of Cordilleran thrust belt in Lima, Montana region. In R. B. Powers (Ed.), *Geologic studies of the Cordilleran thrust belt* (Vol. 1, pp. 137–144). Rocky Mountain Association of Geologists.

Perry, W. J., Jr., Wardlaw, B. R., Bostick, N. H., & Maughan, E. K. (1983). Structure, burial history, and petroleum potential of frontal thrust belt and adjacent foreland, southwest Montana. *The American Association of Petroleum Geologists Bulletin*, *67*(5), 725–743. https://doi.org/10.1306/03B5B6A0-16D1-11D7-8645000102C1865D

Peterson, J. A. (1981). General stratigraphy and regional paleostructure of the western Montana overthrust belt. In *Montana Geological Society field conference & symposium guidebook to southwest Montana* (pp. 5–35). Montana Geological Society.

Pfiffner, O. A. (2006). Thick-skinned and thin-skinned styles of continental contraction. In S. Mazzoli, & W. H. Butler (Eds.), *Styles of continental contraction* (Vol. 414, pp. 153–177). Geological Society of America Special Paper. https://doi.org/10.1130/2006.2414(09

Pfiffner, O. A. (2017). Thick-skinned and thin-skinned tectonics: A global perspective. *Geosciences*, *7*(3), 71. https://doi.org/10.3390/geosciences7030071

Price, R. A. (1981). The Cordilleran foreland thrust and fold belt in the southern Canadian Rocky Mountains. *Geological Society of London*, *9*(1), 427–448. https://doi.org/10.1144/GSL.SP.1981.009.01.39

Price, R. A., & Mountjoy, E. W. (1970). Geologic structure of the Canadian Rocky Mountains between Bow and Athabasca Rivers—A progress report. Structure of the southern Canadian Cordillera (Vol. 6, pp. 7–25). Geological Association of Canada Special Paper.

Ramírez-Peña, C. F., & Chávez-Cabello, G. (2017). Age and evolution of thin-skinned deformation in Zacatecas, Mexico: Sevier orogeny evidence in the Mexican Fold-Thrust Belt. *Journal of South American Earth Sciences*, *76*, 101–114. https://doi.org/10.1016/j.jsames.2017.01.007

Richardson, T., Ridgway, K. D., Gilbert, H., Martino, R., Enkelmann, E., Anderson, M., & Alvarado, P. (2013). Neogene and Quaternary tectonics of the Eastern Sierras Pampeanas, Argentina: Active intraplate deformation inboard of flat-slab subduction. *Tectonics*, *32*(3), 780–796. https://doi.org/10.1002/tect.20054

Rich, J. L. (1934). Mechanics of low-angle overthrust faulting as illustrated by Cumberland Thrust Block, Virginia, Kentucky, and Tennessee. *The American Association of Petroleum Geologists Bulletin*, *18*(12), 1584–1596. https://doi.org/10.1306/3D932C94-16B1-11D7-8645000102C1865D

Rodgers, D. W., & Janecke, S. U. (1992). Chapter 3: Tertiary paleogeologic maps of the western Idaho-Wyoming-Montana thrust belt. In P. K. Link, M. A. Kuntz, & L. B. Piatt (Eds.), *Regional geology of eastern Idaho and western Wyoming* (Vol. 179, pp. 83–94). Geological Society of America Memoir. https://doi.org/10.1130/MEM179-p83

Rosenblume, J. A., Finzel, E. S., & Pearson, D. M. (2021). Early Cretaceous provenance, sediment dispersal, and foreland basin development in southwestern Montana, North American Cordillera. *Tectonics*, *40*, 1–31. https://doi.org/10.1029/2020TC006561

Rose, P. R. (1976). Mississippian carbonate shelf margins, western United States. *Journal of Research of the U. S. Geological Survey*, *4*(4), 449–466.

Ross, C. P. (1934). Correlation and interpretation of Paleozoic stratigraphy in south-central Idaho. *Geological Society of America Bulletin*, *45*(5), 937–1000. https://doi.org/10.1130/GSAB-45-937

Ross, C. P. (1947). Geology of the Borah Peak quadrangle, Idaho. *Geological Society of America Bulletin*, *58*(12), 1085–1160. https://doi.org/10.1130/0016-7606(1947)58[1085:GOTBPQ]2.0.CO;2

Royse, F., Jr., Warner, M. T., & Reese, D. L. (1975). Thrust belt structural geometry and related stratigraphic problems Wyoming-Idaho-Northern Utah. Rocky Mountain Association of Geologists.

Ruh, J. B., Kaus, B. J. P., & Burg, J.-P. (2012). Numerical investigation of deformation mechanics in fold-and-thrust belts: Influence of rheology of single and multiple décollements. *Tectonics*, *31*(3). https://doi.org/10.1029/2011TC003047

Ruppel, E. T. (1968). *Geologic map of the Leadore quadrangle, Lemhi County, Idaho* (GQ-733, scale 1:62,500). U.S. Geological Survey.

Ruppel, E. T. (1986). The Lemhi Arch: A late Proterozoic and early Paleozoic landmass in Central Idaho. In J. A. Peterson (Ed.), *Paleotectonics and sedimentation in the Rocky Mountain Region, United States* (Vol. 41, pp. 119–130). American Association of Petroleum Geologists. https://doi.org/10.1306/M41456C6

Ruppel, E. T., & Lopez, D. A. (1988). Regional geology and mineral deposits in and near the central part of the Lemhi Range, Lemhi County, Idaho. *US Geological Survey Bulletin*, *1480*.

Ryder, R. T., & Scholten, R. (1973). Syntectonic conglomerates in southwestern Montana: Their nature, origin, and tectonic significance. *Geological Society of America Bulletin*, *84*(3), 773–796. https://doi.org/10.1130/0016-7606(1973)84<773:SCISMT>2.0.CO;2

Saleeby, J. (2003). Segmentation of the Laramide Slab-evidence from the southern Sierra Nevada region. *Geological Society of America Bulletin*, *115*(6), 655–668. https://doi.org/10.1130/0016-7606(2003)115<0655:SOTLSF>2.0.CO;2

Scheevel, J. R. (1983). Horizontal compression and a mechanical interpretation of Rocky Mountain Foreland Deformation. In W. W. Boberg (Ed.), *Geology of the Bighorn Basin* (pp. 53–62). Wyoming Geological Association.

Schmidt, C. J., Astini, R. A., Costa, C. H., Gardini, C. E., Kraemer, P. E., Tankard, A. J., et al. (1995). Cretaceous rifting, alluvial fan sedimentation, and Neogene inversion, southern Sierras Pampeanas, Argentina. *AAPG Memoir*, *62*. 341. https://doi.org/10.1306/M62593C16

Schmidt, C. J., & Garihan, J. M. (1983). Laramide tectonic development of the Rocky Mountain foreland of southwestern Montana. In J. D. Lowell (Ed.), *Rocky Mountain foreland basins and uplifts* (pp. 271–294). Rocky Mountain Association of Geologists.

Schmidt, C. J., O'Neill, J. M., & Brandon, W. C. (1988). Influence of Rocky Mountain foreland uplifts on the development of the frontal fold and thrust belt, southwestern Montana. In C. J. Schmidt, & W. J. Perry (Eds.), *Interaction of the Rocky Mountain foreland and the Cordilleran thrust belt* (Vol. 17, pp. 171–202). Geological Society of America Memoir. https://doi.org/10.1130/MEM17110.1130/mem171-p171

Schmidt, C. J., & Perry, W. J. (1988). Interaction of the Rocky Mountain foreland and the Cordilleran thrust belt (Vol. 171). Geological Society of America Memoir. https://doi.org/10.1130/MEM171

Scholten, R. (1957). Paleozoic evolution of the geosynclinal margin north of the Snake River Plain, Idaho-Montana. *Geological Society of America Bulletin*, *68*(2), 151–170. https://doi.org/10.1130/0016-7606(1957)68[151:PEOTGM]2.0.CO;2

Scholten, R. (1982). Continental subduction in the northern US Rockies—A model for back-arc thrusting in the western cordillera. In R. B. Powers (Ed.), *Geologic studies of the Cordilleran thrust belt* (Vol. 1, pp. 123–136). Rocky Mountain Association of Geologists.

Scholten, R., & Hait, M. H., Jr. (1962). Devonian System from shelf edge to geosyncline, southwestern Montana-central Idaho. *Paper presented at the Thirteenth Annual Field Conference, Three Forks – Belt Mountains Area, and Symposium: The Devonian System of Montana and Adjacent Areas, September 5–8, 1962* (pp. 13–22). Billings Geological Society.

Scholten, R., Keenmon, K. A., & Kupsch, W. O. (1955). Geology of the Lima region, southwestern Montana and adjacent Idaho. *Geological Society of America Bulletin*, *66*(4), 345–404. https://doi.org/10.1130/0016-7606(1955)66[345:GOTLRS]2.0.CO;2

Scholten, R., & Ramspott, L. D. (1968). Tectonic mechanisms indicated by structural framework of Central Beaverhead Range Idaho Montana (Vol. 105). Geological Society of America Special Paper.

Schwartz, R. K. (1982). Broken Early Cretaceous foreland basin in southwestern Montana: Sedimentation related to tectonism. In R. B. Powers (Ed.), *Geologic studies of the Cordilleran thrust belt* (Vol. 1, pp. 159–183). Rocky Mountain Association of Geologists.

Shannon, J. P., Jr. (1961). Upper Paleozoic stratigraphy of east-central Idaho. *Geological Society of America Bulletin*, *72*(12), 1829–1836. https://doi.org/10.1130/0016-7606(1961)72[1829:UPSOEI]2.0.CO;2

Sherkati, S., Letouzey, J., & Frizon De Lamotte, D. (2006). Central Zagros fold-thrust belt (Iran): New insights from seismic data, field observation, and sandbox modeling. *Tectonics*, *25*(4). https://doi.org/10.1029/2004TC001766

Simpson, G. D. H. (2010). Influence of the mechanical behaviour of brittle-ductile fold-thrust belts on the development of foreland basins. *Basin Research*, *22*(2), 139–156. https://doi.org/10.1111/j.1365-2117.2009.00406.x

Skipp, B. (1988). Cordilleran thrust belt and faulted foreland in the Beaverhead Mountains, Idaho and Montana. In J. Schmidt, & W. J. Perry (Eds.), *Interaction of the Rocky Mountain foreland and the Cordilleran thrust belt* (Vol. 171, pp. 237–266). Geological Society of America Memoir. https://doi.org/10.1130/MEM171-p237

Skipp, B., & Hait, M. H., Jr. (1977). Allochthons along the northeast margin of the Snake River Plain, Idaho. In E. L. Heisey, D. E. Lawson, E. R. Norwood, P. H. Wach, & L. A. Hale (Eds.), *Rocky Mountain thrust belt geology and resources; 29th annual field conference guidebook* (pp. 499–515). Wyoming Geological Association.

Sloss, L. L. (1954). Lemhi Arch, a mid-Paleozoic positive element in south-central Idaho. *Geological Society of America Bulletin*, *65*(4), 365–368. https://doi.org/10.1130/0016-7606(1954)65[365:LAAMPE]2.0.CO;2

Smithson, S. B., Brewer, J. A., Kaufman, S., Oliver, J. E., & Hurich, C. A. (1979). Structure of the Laramide Wind River uplift, Wyoming, from COCORP deep reflection data and from gravity data. *Journal of Geophysical Research*, *84*(B11), 5955–5972. https://doi.org/10.1029/JB084iB11p05955

Staatz, M. H., Sharp, B. J., & Hetland, D. L. (1979). Geology and mineral resources of the Lemhi Pass thorium district, Idaho and Montana: A description of the distribution, geologic setting, mineralogy, and chemistry of the thorium veins in the Lemhi Pass District. *U. S. Geological Survey Professional Paper*, *1049-A*, 1–98.

Stearn, C. W. (1997). Intraspecific variation, diversity, revised systematics and type of the Devonian stromatoporoid, Amphipora. *Palaeontology*, *40*, 833–854.

Stock, C. W. (1990). Biogeography of the Devonian stromatoporoids. *Geological Society of London*, *12*(1), 257–265. https://doi.org/10.1144/gsl.mem.1990.012.01.24

Stockmal, G. S., Beaumont, C., Nguyen, M., & Lee, B. (2007). Mechanics of thin-skinned fold-and-thrust belts: Insights from numerical models. In J. W. Sears, T. A. Harms, & C. A. Evenchick (Eds.), *Whence the mountains? Inquiries into the evolution of orogenic systems: A volume in honor of Raymond A. Price* (Vol. 433, pp. 63–98). Geological Society of America Special Paper. https://doi.org/10.1130/2007.2433(0410.1130/2007.2433(04)

Suppe, J. (1983). Geometry and kinematics of fault-bend folding. *American Journal of Science*, *283*(7), 684–721. https://doi.org/10.2475/ajs.283.7.684

Suppe, J., & Namson, J. (1979). Fault-bend origin of frontal folds of the western Taiwan fold-and-thrust belt. *Petroleum Geology of Taiwan*, *16*, 1–18.

Tavani, S., Granado, P., Corradetti, A., Camanni, G., Vignaroli, G., Manatschal, G., et al. (2021). Rift inheritance controls the switch from thin- to thick-skinned thrusting and basal décollement re-localization at the subduction-to-collision transition. *Geological Society of America Bulletin*, 1–14. https://doi.org/10.1130/B35800.1

Tysdal, R. G. (1988). Deformation along the northeast side of Blacktail Mountains salient, southwestern Montana. In J. Schmidt, & W. J. Perry (Eds.), *Interaction of the Rocky Mountain foreland and the Cordilleran thrust belt* (Vol. 171, pp. 203–216). Geological Society of America Memoir. https://doi.org/10.1130/MEM171-p203

Tysdal, R. G. (2002). Structural geology of western part of Lemhi Range, east-central Idaho. *U. S. Geological Survey Professional Paper*, *1659*, 1–33.

VanDenburg, C. J. (1997). *Cenozoic tectonic and paleogeographic evolution of the Horse Prairie half graben, southwest Montana* (MS thesis). Utah Sate University.

Vollmer, F. W. (1990). An application of eigenvalue methods to structural domain analysis. *Geological Society of America Bulletin*, *102*(6), 786–791. https://doi.org/10.1130/0016-7606(1990)102<0786:AAOEMT>2.3.CO;2

Von Hagke, C., & Malz, A. (2018). Triangle zones – Geometry, kinematics, mechanics, and the need for appreciation of uncertainties. *Earth-Science Reviews*, *177*, 24–42. https://doi.org/10.1016/j.earscirev.2017.11.003

Weil, A. B., Yonkee, A., & Kendall, J. (2014). Towards a better understanding of the influence of basement heterogeneities and lithospheric coupling on foreland deformation: A structural and paleomagnetic study of Laramide deformation in the southern Bighorn Arch, Wyoming. *Geological Society of America Bulletin*, *126*(3–4), 415–437. https://doi.org/10.1130/B30872.1

Weil, A. B., Yonkee, A., & Schultz, M. (2016). Tectonic evolution of a Laramide transverse structural zone: Sweetwater Arch, south central Wyoming. *Tectonics*, *35*(5), 1090–1120. https://doi.org/10.1002/2016TC004122

Weil, A. B., & Yonkee, W. A. (2012). Layer-parallel shortening across the Sevier fold-thrust belt and Laramide foreland of Wyoming: Spatial and temporal evolution of a complex geodynamic system. *Earth and Planetary Science Letters*, *357–358*, 405–420. https://doi.org/10.1016/j.epsl.2012.09.021

White, S. H., Burrows, S. E., Carreras, J., Shaw, N. D., & Humphreys, F. J. (1980). On mylonites in ductile shear zones. *Journal of Structural Geology*, *2*(1–2), 175–187. https://doi.org/10.1016/0191-8141(80)90048-6

Williams, C. A., Connors, C., Dahlen, F. A., Price, E. J., & Suppe, J. (1994). Effect of the brittle-ductile transition on the topography of compressive mountain belts on Earth and Venus. *Journal of Geophysical Research*, *99*(B10), 19947–19974. https://doi.org/10.1029/94JB01407

Williams, S. A., Singleton, J. S., Prior, M. G., Mavor, S. P., Cross, G. E., & Stockli, D. F. (2020). The early Palaeogene transition from thin-skinned to thick-skinned shortening in the Potosí uplift, Sierra Madre Oriental, northeastern Mexico. *International Geology Review*, *63*, 233–263. https://doi.org/10.1080/00206814.2020.1805802

Wiltschko, D. V., & Dorr, J. A. (1983). Timing of deformation in overthrust belt and foreland of Idaho, Wyoming, and Utah. *American Association of Petroleum Geologists Bulletin*, *67*(8), 1304–1322. https://doi.org/10.1306/03B5B740-16D1-11D7-8645000102C1865D

Witte, J., & Oncken, O. (2020). Uncertainty quantification in section-balancing using Pseudo-3D forward modeling – Example of the Malargüe Anticline, Argentina. *Journal of Structural Geology*, *141*, 104189. https://doi.org/10.1016/j.jsg.2020.104189

Worthington, L. L., Miller, K. C., Erslev, E. A., Anderson, M. L., Chamberlain, K. R., Sheehan, A. F., et al. (2016). Crustal structure of the Bighorn Mountains region: Precambrian influence on Laramide shortening and uplift in north-central Wyoming. *Tectonics*, *35*(1), 208–236. https://doi.org/10.1002/2015TC003840

Yang, K. M., Huang, S. T., Wu, J. C., Lee, M., Ting, H. H., & Mei, W. W. (2001). The characteristics of sub-surface structure and evolution of the Tachienshan-Chukou thrust system. *Annual Meeting of the Geological Society of China*, 82–84.

Yeck, W. L., Sheehan, A. F., Anderson, M. L., Erslev, E. A., Miller, K. C., & Siddoway, C. S. (2014). Structure of the Bighorn Mountain region, Wyoming, from teleseismic receiver function analysis: Implications for the kinematics of Laramide shortening. *Journal of Geophysical Research: Solid Earth*, *119*(9), 7028–7042. https://doi.org/10.1002/2013JB010769

Yonkee, A., & Weil, A. B. (2010). Reconstructing the kinematic evolution of curved mountain belts: Internal strain patterns in the Wyoming salient, Sevier thrust belt, U.S.A. *Geological Society of America Bulletin*, *122*(1–2), 24–49. https://doi.org/10.1130/B26484.1

Yonkee, W. A. (1992). Basement-cover relations, Sevier orogenic belt, northern Utah. *Geological Society of America Bulletin*, *104*(3), 280–302. https://doi.org/10.1130/0016-7606(1992)104<0280:BCRSOB>2.3.CO;2

Yonkee, W. A., & Weil, A. B. (2015). Tectonic evolution of the Sevier and Laramide belts within the North American Cordillera orogenic system. *Earth-Science Reviews*, *150*, 531–593. https://doi.org/10.1016/j.earscirev.2015.08.001

Zawislak, R. L., & Smithson, S. B. (1981). Problems and interpretation of COCORP deep seismic reflection data, Wind River Range, Wyoming. *Geophysics*, *46*(12), 1684–1701. https://doi.org/10.1190/1.1441176

Zhou, Y., Murphy, M. A., & Hamade, A. (2006). Structural development of the Peregrina-Huizachal anticlinorium, Mexico. *Journal of Structural Geology*, *28*(3), 494–507. https://doi.org/10.1016/j.jsg.2005.11.005